ENERGY CARRIER TRANSPORT IN SURFACE-MODIFIED CARBON NANOTUBES

A Dissertation

by

Yeontack Ryu

Submitted to the Office of Graduate Studies of
Texas A&M University
in partial fulfillment of the requirements for the degree of

DOCTOR OF PHILOSOPHY

Approved by:

Chair of Committee,	Choongho Yu
Committee Members,	Kalyan Annamalai
	Hong Liang
	Perla Beatriz Balbuena
Head of Department,	Jerald Caton

December 2012

Major Subject: Mechanical Engineering

ABSTRACT

Carbon nanotubes are made into films or bulks, their surface or junction morphology in the networks can be modified to obtain desired electrical transport properties by various surface modification methods. The methods include incorporation of organic molecules or inorganic nanoparticles, debundling of nanotubes by dispersing agents, and microwave irradiation. Because carbon nanotubes have unique carrier transport characteristics along a sheet of graphite in a cylindrical shape, the properties can be dramatically changed by the modification. This is ideal for developing high-performance materials for thermoelectric and photovoltaic energy conversion applications. In this research, decoration of various organic/inorganic nanomaterials on carbon nanotubes was employed to enhance their electrical conductivity, to improve thermoelectric power factor by modulating their electrical conductance and thermopower, or to obtain n-type converted carbon nanotube. The electrical conductivity of double-wall nanotubes (DWNTs) decorated with tetrafluoro-tetracyanoquinodimethane (F_4TCNQ) was increased up to 5.9×10^5 S/m. The sheet resistances were measured to be 42 Ω/sq at 75% of transmittance for $HNO_3/SOCl_2$-treated DWNT films, making their electrical conductivities 200~300% better than those of the pristine DWNT films. A series of experiments at different ion concentrations and reaction time periods were systematically performed in order to find optimum nanomaterial formation conditions and corresponding electronic transport changes for better thermoelectric power factor. For example, the thermoelectric power factors were improved by ~180% with F_4TCNQ

on DWNTs, ~200% with Cu on SWNTs, and ~140% with Fe on single-walled nanotubes (SWNTs). Also SWNTs was converted from p-type to n-type with a large thermopower (58 μV/K) by using polyethyleneimine (PEI) without vacuum or controlled environment. This transport behavior is believed to be from charge interactions resulted from the difference between the work functions/reduction potentials of nanotubes and nanomaterials. In addition, different dispersing agents were utilized with DWNT and SWNTs to see a debundling effect in a film network. The highest electrical conductivity of ~1.72×10^{6} S/m was obtained from DWNT film which was fabricated with a nanotube solution dispersed by chlorosulfonic acid. Debundling of nanotubes in the film network has been demonstrated to be a critical parameter in order to get such high electrical property. In the last experiment, Au nanoparticle decoration on carbon nanotube bundle was performed and a measurement of themophysical properties has done before and after modifying carbon nanotube surface. Carbon nanotube bundle, herein, was bridged on microdevice to enable the measurement work. This study demonstrates a first step toward a breakthrough in order to extract the potential of carbon nanotubes regarding electron transport properties.

DEDICATION

To my parents Sunkgu Ryu and Aeja Lee, my wife Ahram Lee, and my daughter Minseo Ryu for their endless support

ACKNOWLEDGEMENTS

I would like to thank my committee chair, Dr. Choongho Yu, and my committee members, Dr. Kalyan Annamalai, Dr. Hong Liang, and Dr. Perla Beatriz Balbuena for their guidance and support throughout the course of this research.

Thanks also go to my friends and colleagues and the department faculty and staff for making my time at Texas A&M University a great experience.

I would like to thank to National Science Foundation (NSF) for sponsoring the research project for my Ph.D. dissertation. During the completion of my Ph.D. dissertation at Texas A&M University – I was also supported from the following research projects managed by Dr. Yu at the Texas Engineering Experiment Station (TEES) – which I gratefully acknowledge: U.S. Air Force Office of Scientific Research (Grant No. FA9550-09-1-0609) under the auspices of Dr. Charles Lee; U.S. National Science Foundation (Grant No. CMMI 1030958); Pioneer Research Center Program through the National Research Foundation of Korea (Grant No. 2010-0002231) funded by the Ministry of Education, Science and Technology (MEST).

In addition, I would like to appreciate my colleagues; Kyungwho Choi, Hongjoo Yang, Liang Yin, Pu Xiong, and Abdullah Tazebay; for their friendship and support.

I really thank my mother and father for their love and support. I also thank my wife Ahram Lee and my daughter Minseo Ryu who give me strength and inspiration. It would not be possible to complete my graduate work without their sacrifice, patience, support, belief, and love.

Finally, I am grateful to everyone who has helped me in some way or another throughout this entire duration.

NOMENCLATURE

A	Cross-sectional area of a sample (m^2)
$D(E)$	Electronic density of states
e	Electron charge (coulombs)
E	Energy
E^0	Standard electrode potential (eV)
E_f	Fermi level
E_m	Mean energy
f_{ED}	Fermi-Dirac distribution
G_e	Electrical conductance ($1/\Omega$)
G_t	Thermal conductance (W/K)
T	Temperature (K)
L	Length of a sample (m)
n	Number density of carrier
Q	Heat energy (W)
q	Carrier charge (coulombs)
S	Seebeck coefficient or thermopower (V/K)
Z	Thermoelectric efficiency
Z_0	Impedence of free space

Greek Symbols

κ	Thermal conductivity (W/mK)
μ	Carrier mobility
σ	Electrical conductivity (S/m)
σ_{op}	Optical conductivity
$\psi(E)$	Differential electrical conductivity

TABLE OF CONTENTS

Page

LIST OF FIGURES

Page

LIST OF TABLES

Page

1. INTRODUCTION

Carbon occupies four electrons in its outer valence shell and they have $2s^2$ $2p^2$ in configuration of the ground state. Graphite, diamond, and carbon nanotube (CNT) are considered as typical forms pure carbon. Graphite presents sp^2 hybridization where each atom is located in a single plane forming 120° between the atoms, and also has p_z orbital along z direction responsible for a weak bonding called as a van der Waals bond. The sp^2 bonds between carbon atoms form honeycomb lattice structure considered as a typical graphite sheet. The free electrons from the p_z orbital are active in the cloud and can be delocalized to a single carbon atom. This is why graphite is conductive. On the contrary, diamond shows sp^3 hybridization where four carbon atoms are connected with 109.5° between them forming a regular tetrahedron. The structure with highly directed charge density between carbons forms extremely rigid bonds and makes it electrically resistive. Carbon nanotubes can be visualized as a sheet of graphite which has been rolled into a tube shape. When the graphite sheet is rolled up to form the nanotube, the orbital structure is altered because the bond length and angle are changed. First, σ and π orbitals are overlapped both inside and outside of the tube. A continuous ring inside shows σ characteristic, while wavefuntions outside present rearrangement of π orbitals. This phenomenon, rehybridization, induces a mixture of sp^2 and sp^3 orbitals in carbon nanotubes. There are two types of carbon tubes: single-walled (SWNTs) and multi-walled (MWNTs).

In this study, various nanomaterials are incorporated into carbon nanotube surface. Such chemisorption of nanomaterials can give an influence on electrical and thermal properties. First, a phonon scattering may occur due to a mass difference between carbon and nanomaterial. Because thermal conductivity described by Boltzmann transport equation is proportional to relaxation time which has an inverse relation with a phonon scattering, the increase of scattering results in reduction of thermal conductivity. In addition, the scattering can also decrease electron mobility because the mobility is also proportional to relaxation time. Electrical conductivity is defined as $\sigma = nq\mu$ where n, q, and μ respectively indicate number density, charge, and mobility of carrier in solid state physics. Thus, σ can be increased or decreased by n or μ. Even though a reduction of carrier mobility is expected due to the scattering in incorporation of nanomaterials, number density of carrier is likely to be more dominant in terms of electrical conductivity so that the change of mobility can be ignored.

This dissertation consists of five experiments which contribute to demonstrate the unique energy carrier transport phenomena in low dimensional carbon nanotube structure as well as to improve the transport properties for renewable energy harvesting such as photovoltaics and thermoelectric. This chapter describes the motivation of five experiments.

1.1. Effect of metal nanopaticles decoration on thermoelectric power factor in one dimensional carbon nanotube structure

Carbon nanotubes have excellent intrinsic electrical properties, which are very promising for many applications including thermoelectrics,[1-4] nanoelectronics,[5] and photovoltaics.[6,7] Furthermore, they are very sensitive to external disturbances, making them ideal for sensing tiny species.[8] Furthermore, when nanotubes are made into films or bulks, junctions between nanotubes can be modified to obtain desired electrical and thermal transport properties.[3] Such dramatic changes are caused by their unique carrier transport characteristics along a sheet of graphite in a cylindrical shape. The unique transport characteristics provide great opportunities of manipulating electronic transport properties. For instance, this is essential to synthesizing efficient thermoelectric materials, which require high electrical conductivity and thermopower (or the Seebeck coefficient) with low thermal conductivity. A measure of thermoelectric efficiency (Z) is often described as $Z = S^2\sigma/k$, where S, σ, and k respectively stand for thermopower, electrical conductivity, and thermal conductivity.[9] In typical bulk materials, strong correlations between these parameters make Z improvement extremely difficult. For example, an increase of hampers S, resulting in a small change of $S^2\sigma$ (called as the power factor). In general, in order to achieve a large power factor, it is necessary to have a large anisotropy such as narrow sharp bands in the electronic density of states.[10] Carbon nanotubes whose electronic density of states has spike-shape Van Hove singularities are excellent for this purpose. The Fermi level of nanotubes can be readily altered by using impurities such as nanoparticles and molecules.

1.2. Decoration of organic/inorganic nanomaterials on carbon nanotubes yielding high electrical conductivity or n-type thermopower

Carbon nanotubes have unique electron and phonon transport characteristics due to their hollow cylindrical-shape structures, which make transport properties susceptible to external disturbances.[11] These characteristics make it possible to change the properties dramatically, which is ideal for developing high-performance materials for thermoelectric and photovoltaic energy conversion applications. For example, nanotube films are promising for the use of transparent and electrically-conducting electrodes. Both p- and n-type nanotubes can be electrically connected in series for the operation of thermoelectric energy harvesting or refrigeration.[1-3] In order to have efficient thermoelectrics, it is necessary to achieve high electrical conductivity and large thermopower that comprise the thermoelectric figure of merit, $ZT = S^2\sigma T/k$, where S, σ, T, and k are respectively thermopower, electrical conductivity, absolute temperature, and thermal conductivity.[9] A high $S^2\sigma$ (known as the thermoelectric power factor) and a low k are necessary to have a large ZT at a given temperature. In general, a simultaneous increase of S and σ in typical semiconductors is very difficult, but it is feasible to alleviate such strong correlation in low-dimensional materials due to the spike-like shape electronic density of states (e.g., Van Hove singularity). When the Fermi level of nanotubes is located near the spike-like shape density of states as a result of charge transfer between nanotubes and nanomaterials incorporated into nanotubes, extraordinary transport phenomena can be observed.

1.3. Effect of decorating nanomaterials on transparent and conductive carbon nanotube films

Optically transparent and electrically conductive materials are widely used in many electronic devices such as touch-screens, solar cell electrodes, and a variety of electronic displays. Indium-tin oxide (ITO) has been popular for these applications, but indium is getting more expensive due to its scarcity on earth. Carbon nanotube films could be an excellent substitute for ITO because of their high electrical conductivity, abundance of carbon, mechanical flexibility, and relatively easy solution-based fabrication. Several different methods such as acid treatment and nanoparticle decoration have been employed to improve electrical properties of the carbon nanotube films.[11-15] These methods often utilize doping that increases carrier concentrations although nanotube dispersion[16,17] or defects on nanotubes[18,19] may also affect the electrical properties of nanotube films.

1.4. Effect of debundling and hole-doping in carbon nanotube films

Individual carbon nanotubes have excellent electrical properties for various applications including energy conversion and electronics, but the properties are often significantly altered when the nanotubes are bundled. Unfortunately, as-synthesized nanotubes are typically bundled and extremely difficult to individually separate them. This makes it difficult to utilize their extraordinary intrinsic properties due to the presence of contact junctions in bulk or film samples. When nanotubes are individually separated, bulks or films are expected to show very high conductivity. This is because the electrical conduction, which is often limited by tube-tube junctions, can be improved

by increasing the number of the junctions (i.e., more electron transporting channels). In practice, carbon nanotubes are used in a form of bundles, mats, or bulks rather than a single individual tube. Therefore, it is very important to study the properties of nanotubes when they are in such forms. For example, a high electrical conductivity of a carbon nanotube film is desirable for flexible solar cell electrodes,[20,21] thermoelectrics,[1,3,11,15,22] and battery electrodes.[23,24]

1.5. Thermal and electrical measurement in nanoparticle decorated carbon nanotube bundle

Low dimensional nanomaterials have unique charge transfer properties which may lead to enhancement of thermoelectric energy conversion. Especially, carbon nanotube individual or bundle has been known to be superior in electrical and thermal conductivities. But the properties are typically reduced much when they are fabricated as bulk materials like films or mats. It is of interest to investigate junction properties between nanotubes or surface-modified nanotubes. In previous studies, thermoelectric properties have been analyzed for variously surface-modified carbon nanotube films. Now it is necessary to confirm such property changes in a small scale of carbon nanotubes. It indicates that nanotube individual or bundles can be utilized to find out nanoparticle decoration effect. In addition to electrical conductance and Seebeck coefficient, thermal conductance is able to be measured in this experiment. Eventually, those three properties will provide *ZT*, a figure of merit in thermoelectric, so that carbon nanoutbes can be used with larger understanding in field of energy harvesting.

1.6. Overview

Carbon nanotubes have excellent intrinsic electrical properties, which are very promising for many applications including thermoelectrics, nanoelectronics, and photovoltaics. Furthermore, they are very sensitive to external disturbances, making them ideal for sensing tiny species. When they are made into films or bulks, their surface or junction morphology in the networks can be modified to obtain desired electrical transport properties by various surface modification methods. The methods include incorporation of organic molecules or inorganic nanoparticles, debundling of nanotubes by dispersing agents, and microwave irradiation. Because carbon nanotubes have unique carrier transport characteristics along a sheet of graphite in a cylindrical shape, the properties can be dramatically changed by the modification. This is ideal for developing high-performance materials for thermoelectric and photovoltaic energy conversion applications. In this research, decoration of various organic/inorganic nanomaterials on carbon nanotubes was employed to enhance their electrical conductivity, to improve thermoelectric power factor by modulating their electrical conductance and thermopower, or to obtain n-type converted carbon nanotube. Single-wall (SWNTs) or double-wall nanotubes (DWNTs) were made into films by spraying nanotube solutions on glass substrates, and then the films were immersed in different concentrations of each solution containing the nanomaterials for various time periods. The electrical conductivity of DWNTs decorated with tetrafluoro-tetracyanoquinodimethane (F_4TCNQ) was increased up to 5.9×10^5 S/m. The sheet resistances were measured to be 42 Ω/sq at 75 % of transmittance for $HNO_3/SOCl_2$-treated DWNT films and 64 Ω/sq at 77 % for Au-

decorated DWNT films, making their electrical conductivities 200~300 % better than those of the pristine DWNT films. A series of experiments at different ion concentrations and reaction time periods were systematically performed in order to find optimum nanomaterial formation conditions and corresponding electronic transport changes for better thermoelectric power factor. For example, the thermoelectric power factors were improved by ~180% with F_4TCNQ on DWNTs, ~200% with Cu on SWNTs, and ~140% with Fe on SWNTs. Also SWNTs was converted from p-type to n-type with a large thermopower (58 μV/K) by using polyethyleneimine (PEI) without vacuum or controlled environment. This transport behavior is believed to be from charge interactions resulted from the difference between the work functions/reduction potentials of nanotubes and nanomaterials. In addition, different dispersing agents were utilized with DWNT and SWNTs to see a debundling effect in a film network. The highest electrical conductivity of $\sim 1.72 \times 10^6$ S/m was obtained from DWNT film which was fabricated with a nanotube solution dispersed by chlorosulfonic acid. Debundling of nanotubes in the film network has been demonstrated to be a critical parameter in order to get such high electrical property. In the near future, measurement study for a nanoparticle decoration will be added here with individual carbon nanotube or bundle bridged on microdevice. This study demonstrates a first step toward a breakthrough in order to extract the potential of carbon nanotubes regarding electron transport properties.

1.7. Scope of current study

This study is expected to make fundamental contributions to the field of carbon nanotube electronics in the following ways:

- Demonstrate that electrical transport properties of carbon nanotube films can be dramatically altered by decorating nanomaterials on the surface of nanotubes due to large anisotropy shown in one-dimensional carbon nanotube structures

- Fabricate p-type and n-type carbon nanotube conductors with competitive electrical properties and provide the thermoelectric information to polymer-composite so that the nanotubes can be used as good fillers.

- Understand charge transfer between nanotubes and various nanomaterials including both organic and inorganic materials and identify good materials which can be effectively utilized in energy conversion.

- Evaluate the effect of various parameters such as nanomaterial concentration, size, density, and nannotube morphology, and optimize those in order to have the most desirable outcomes.

- Fabricate transparent and conductive carbon nanotube films for substituting indium-tin oxide (ITO) in solar cell application. Depending on the improved

electrical properties of surface-modified carbon nanotubes, identify the minimum sheet resistance value in transparent and conductive electrode using carbon nanotubes.

- Provide direct evidence regarding energy transport in nanoparticle decorated carbon nanotubes by measuring electrical and thermal properties of nanotube bundle.

2. STUDY 1: MODULATING ELECTRONIC TRANSPORT PROPERTIES OF CARBON NANOTUBES TO IMPROVE THE THERMOELECTRIC POWER FACTOR VIA NANOPARTICLE DECORATION[*]

A spraying method was employed to prepare carbon nanotube thin films and home-made four probe method was utilized to measure the resistance and Seebeck coefficient. Au and Cu nanoparticles were decorated on carbon nanotube films by a spontaneous reduction or a galvanic displacement method. Electrical resistance and Seebeck coefficient of the films were measured before and after the decoration to see how those properties are changed as well as to estimate thermoelectric power factor. This work gives us important information of electron transport phenomena when carbon nanotube network is surface-modified by metal nanoparticle decoration. In addition, it also gives a good contribution to understand unique energy carrier transport in one dimensional carbon nanotube structure.

2.1. Background information

In this study, nanoparticle precipitations on nanotubes were performed by using galvanic displacement or the difference of reduction potentials between nanotubes and reducing agents.[25,26] Figure 2-1 shows schematic drawings of galvanic displacement and

[*] Reprinted with permission from "Modulating Electronic Transport Properties of Carbon Nanotubes To Improve the Thermoelectric Power Factor via Nanoparticle Decoration" by Choongho Yu, Yeontack Ryu, Liang Yin, and Hongjoo Yang, 2011. *ACS Nano*, 5(2), 1927-1303, Copyright [2011] by American Chemical Society.

spontaneous reduction. In case of galvanic displacement, metal ions in a solution were reduced on nanotubes by dissolving another metal whose reduction potential is smaller than that of the reduced metal. Electrons released from the dissolved metal are delivered to the ions in the solution, forming metal nanoparticles on nanotubes. When the reduction potential of ions in a solution is larger than that of nanotubes, nanoparticles are also spontaneously precipitated. The spontaneous reduction method is limited to a few metals such as gold and platinum whereas the galvanic displacement method can be used for obtaining various metal nanoparticles. Charge transfers between nanoparticles and nanotubes as well as structural changes due to particle incorporations may considerably alter transport properties due to modifications of carrier densities, mobilities,[4] and contact junctions.

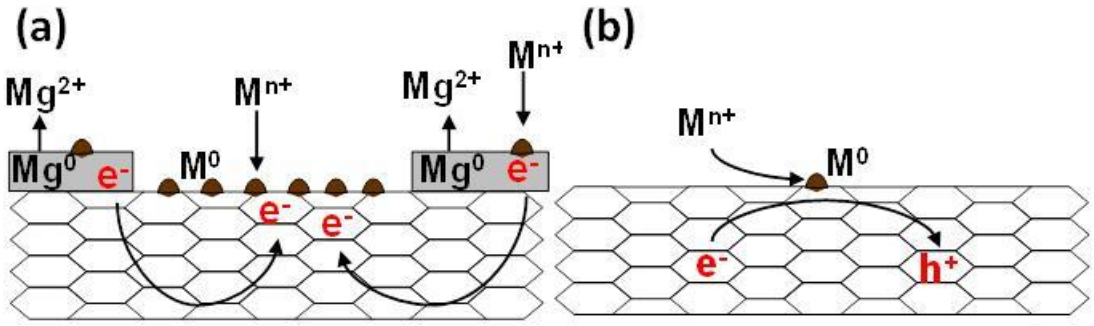

Figure 2-1 Nanoparticle precipitations on nanotubes by galvanic displacement (a) and spontaneous reduction (b). The hexagon arrays represent nanotubes.

In this experiment, 200 % increases in the thermoelectric power factor were observed with copper nanoparticle decorations on nanotubes. Methodologies of manipulating thermopower/electrical conductivity as well as morphologies/structures of nanoparticles upon various reaction conditions were also presented. A series of

experiments at different ion concentrations and reaction time periods were systematically performed in order to find nanoparticle formation conditions that improve the thermoelectric power factor. The following describe experimental procedures, electronic properties upon decorating various density and size nanoparticles on nanotubes as well as discussion regarding transport property changes.

2.2. Experimental procedure

12-mg carbon nanotubes (purified grade nanotubes synthesized by arc discharge method; P2-SWNT, Carbon Solution Inc.) were dispersed in 20-mL deionized (DI) water with 24-mg sodium dodecyl benzene sulfonate (SDBS, Acros organics, 88%) by ultra-sonication for 3 min. Then, the solution was centrifuged at 6000 rpm for 15 min in order to obtain supernatant solution. According to the product information of P2-SWNT, metal contents (Ni, Y) range from 4 to 7 wt% and carbonaceous purity is greater than 90%. Average diameters of individual tubes and bundles are 1.4 and 4-5 nm, respectively. The average length of bundles ranges from 500 nm to 1.5 μm. The solution was sprayed on glass slides at a temperature of ~80 ℃ with a spray gun (Fuso Seiki Co., GP-S1, 0.2 mm nozzle diameter). The thickness of samples was strongly dependent on solution quantity, which was kept the same for all samples in this study. Typical film thicknesses were measured to be 150~200 nm. Then, the samples were immersed into deionized water for 30 min so as to remove SDBS surfactant and subsequently dried by compressed air. The typical size of samples is ~6 mm × 25 mm. Metal ion solutions were prepared by dissolving $CuSO_4$ (Fisher scientific, 99+%) and $HAuCl_4$ (Alfa aesar,

99.9%) in deionized water. The samples were immersed into 1, 10, or 20 mM concentration solutions for various time periods. Thin Electrodes made of a silver paint at the end of the long edge of the samples were used for gold incorporation. Zinc foils were attached to the electrodes of nanotube films by a silver paint for copper incorporation.

Electrical conductance and thermopower were measured at room temperature by using a home-made four-probe setup with two T-type thermocouples and two copper wires. Four silver line-shape electrodes were made on both edges of the samples for the measurements. Then, the samples were placed on a setup that is composed of two thermoelectric devices to create variable temperature difference. A current-voltage (I-V) sweeping method across the long edge of the samples was employed to generate linear I-V curves so as to obtain sample conductance. Voltages between two electrodes at both ends of the samples were measured at 6 different temperature differences between 0~±7 ℃ to extract thermopower. The transport properties were characterized before and after nanoparticle incorporation processes. Film thicknesses were measured by using an optical surface profilometer (Wyko NT9100 optical profiler, Veeco Instruments Inc.). Morphology, structure, and energy dispersive spectroscopy analysis were performed by using a SEM (Quanta 600), a TEM (JEOL JEM-2010), and an X-ray diffractometer (Bruker-AXS D8 VARIO).

2.3. Results and discussion

Nanotubes were fabricated into films by spraying nanotubes dispersed by sodium dodecyl benzene sulfonate (SDBS) in deionized water. The films were immersed in solutions with different copper or gold ion concentrations for various time periods in order to precipitate nanoparticles of different sizes and densities.

In order to attach copper or gold nanoparticles to nanotubes, either zinc or silver electrodes were used for galvanic displacement. Gold reduction potential ($[AuCl_4]^- + 3e^+ \rightarrow Au(s) + 4Cl^-$, standard electrode potential (E^0) = +0.93 V)[27] is larger than silver ($Ag^+ + e^- \rightarrow Ag(s)$, E^0 = +0.7996 V),[27] making gold ions reduced on nanotubes by ionizing silver. Copper reduction potential ($Cu^{2+} + 2e^- \rightarrow Cu(s)$, E^0 = +0.34 V)[27] is close to E^0 (=+0.2 ~ +0.5 V)[28,29] of carbon nanotubes, but is much larger than that of zinc ($Zn^{2+} + 2e^- \rightarrow Zn(s)$, E^0 = -0.7618 V).[27] Note that the Fermi level of nanotubes is typically measured in vacuum environment), but it does change depending on doping such as oxygen for nanotubes exposed to air.[30] The samples were immersed in aqueous solutions of 1 mM, 10 mM, and 20 mM $CuSO_4$ for 30 sec, 3 min, 10 min, 15 min, 30 min, 1 hour 30 min, 3 hours, or 18 hours. Scanning electron micrographs (SEMs) are shown in Figure 2-2 after 30 sec (Figure 2-2(a1), (b1), (c1)), 3 min (Figure 2-2(a2), (b2)), 15 min (Figure 2-2(c2)), or 30 min (Figure 2-2(a3), (b3), (c3)) reactions. Nanoparticles start to precipitates even with the lowest concentration (1 mM) for 30 sec (Figure 2-2(a1)). Particle sizes range from a few nm to a hundred nm (see the image with a 500-nm scale bar in Figure 2-2(d)).

Figure 2-2 Nanotube films after reactions in $CuSO_4$ solutions of the following concentrations for various time period: (a1) 1 mM-30 sec, (a2) 1 mM-3 min, (a3) 1 mM-30 min, (b1) 10 mM-30 sec, (b2) 10 mM-3 min, (b3) 10 mM-30 min, (c1) 20 mM-30 sec, (c2) 20 mM-15 min, (c3) 20 mM-30 min, (d) a portion of (a1) with a higher magnification, (e) a portion of (b1) with a higher magnification, (f) copper nanoparticle (ellipse at the center) attached to nanotube bundles (wavy lines in the horizontal direction), and (g) X-ray diffractions of the sample shown in (b2) (upper black line) and (a3) (lower brown line). The scale bars for (a1)~(c3) represent 2 μm, and those for (d) and (e) 500 nm. Smaller nanoparticles were precipitated after reactions with the low concentration solutions, which provide more surface areas for a given volume of materials.

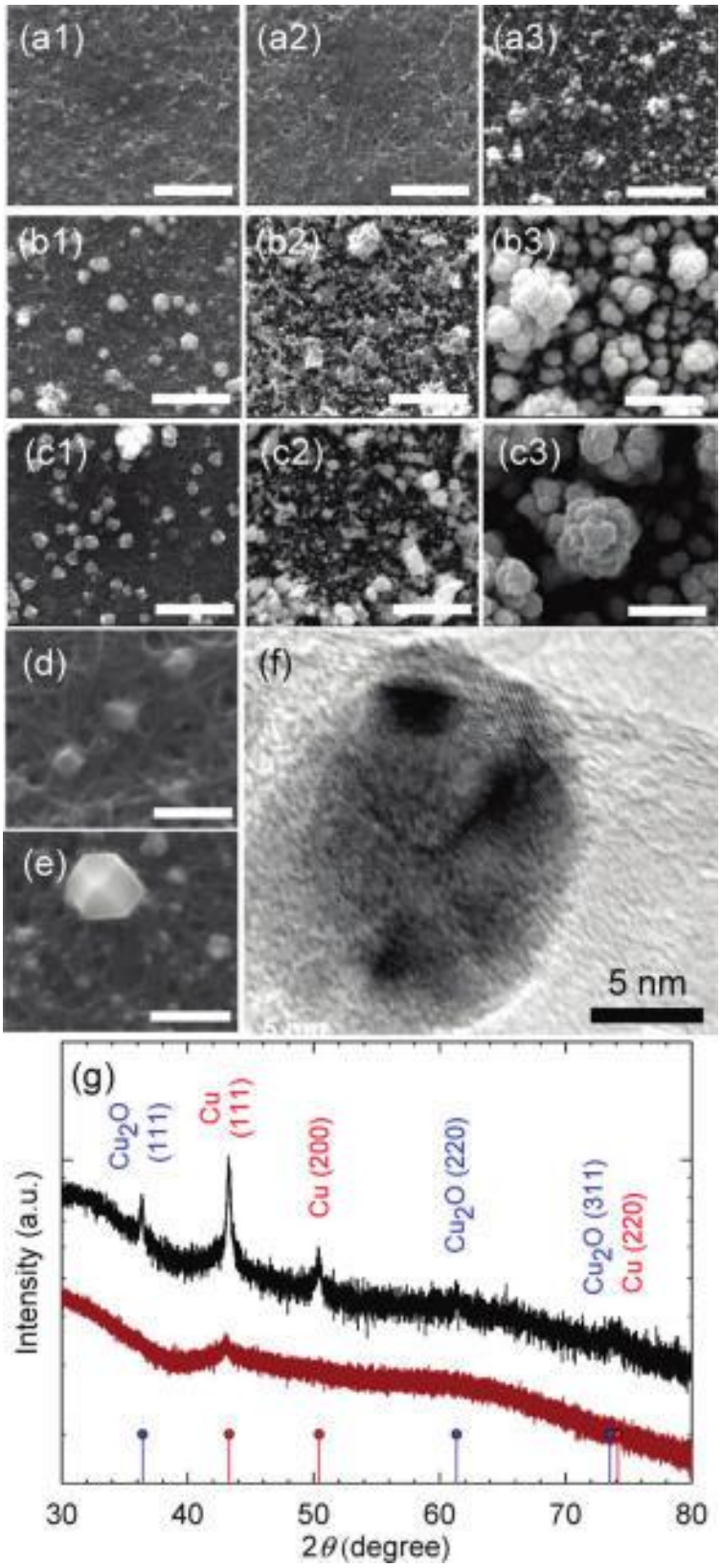
(a1)
(a2)
(a3)
(b1)
(b2)
(b3)
(c1)
(c2)
(c3)
(d)
(e)
(f)
5 nm
(g)
Cu2O (111)
Cu (111)
Cu (200)
Cu2O (220)
Cu2O (311)
Cu (220)
Intensity (a.u.)
30
40
50
60
70
80
2θ (degree)

As the reaction time was increased to 3 min (Figure 2-2(a2)) and 30 min (Figure 2-2(a3)), the size and density of particles were increased. Low ion concentration resulted in slow particle precipitation rates compared to those with high concentrations (compare the 1-mM case (Figure 2-2(a1)) with 10-mM (Figure 2-2(b1)) for 30 sec reactions; compare the 1-mM case (Figure 2-2(a2)) with 10-mM (Figure 2-2(b2)) for 3 min reactions). When high concentration solutions (10 mM and 20 mM) were used, copper nanoparticles coalesced, resulting in relatively large (a few hundred nm) particles. The particles from a high concentration (20 mM) clearly show crystalline faces as indicated in Figure 2-2(e). Images in Figure 2-2(a3) and (b2) respectively from 1 mM-30 min and 10 mM-3 min reactions indicate a lower concentration makes less dense and smaller nanoparticles. A long period reaction with a high concentration such as 20 mM-30 min reaction in Figure 2-2(c3) formed a continuous layer of nanoparticles. A transmission electron micrograph of a sample with a 1 mM-30 min copper reaction shows crystalline nanoparticles attached to nanotube bundles, as shown in Figure 2-2(f). Lattice patterns are shown in the particle (dark ellipse) and nanotube bundles are shown as wavy lines in the horizontal direction. X-ray diffraction patterns of samples (Figure 2-2(g)) after 1 mM-30 min (lower plot, brown color) and 10 mM-3 min (upper plot, black color) reactions indicate that the reaction with a higher concentration is easier to crystallize copper than that with a lower concentration. The crystalline Cu_2O may have formed during the experiments since the sample was exposed to water and air. In general, O_2 dissolved in the water-based solution is dissociated upon reaction with copper and then forms Cu_2O unless the reaction occurs at high temperatures.[31] Since the oxidation

process do not involve charge transfer between nanotubes and copper (or Cu_2O), the oxidation is not likely to have significant influence on changing carrier concentrations in nanotubes.

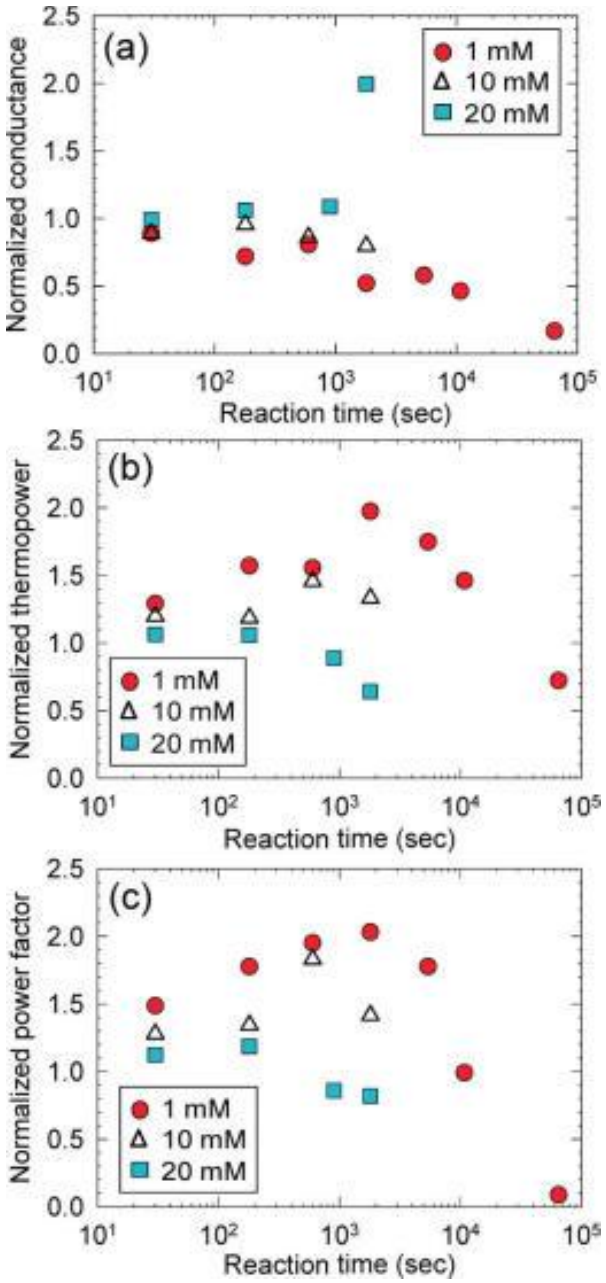

Figure 2-3 Normalized conductance (a), thermopower (b), and the power factor (c) after reactions in 1, 10, and 20 mM $CuSO_4$ solutions as a function of reaction time. Reactions in 1 mM solution resulted in 200 % increase of the power factor.

Electrical conductance and thermopower measurement results are plotted in Figure 2-3(a) and (b), and the power factors were calculated (Figure 2-3(c)). All properties were normalized by those of samples prior to metal-decoration processes. Note that the initial conductance/thermopower as well as film thicknesses (150-200 nm) was similar. In addition, metal ions can access to nanotubes located at both outer and inner parts of the films due to numerous voids between tangled nanotubes (see micrographs in Figure 2-2). For 1 and 10 mM reactions, the electrical conductance was decreased with increasing reaction time. On the contrary, the reaction with 20 mM for 30 min suddenly doubled conductance. This is because the dense copper particles, shown in Figure 2-2(c3), are likely to be electrically connected. The electrical conductivity of bulk copper (~6×10^7 S/m at 300 K)[32] is typically one- or two-order higher than those of carbon nanotube films. Note that the intrinsic electrical conductivity of nanotubes is up to ~2×10^7 S/m at room temperature,[33] but electron transport is hampered by contact resistance between nanotubes in films and bulks. Electrical conductivity and thermopower of as-synthesized films in this study are measured to be 5×10^4~10^5 S/m and 25~30 μV/K at 300 K. The significant reduction from 1 to 0.64 for the normalized thermopower after a 20 mM-30 min reaction (blue square, shown in Figure 2-3(b)) would imply that copper have participated in electron transport. Note that thermopower of copper is small (1.83 μV/K at 300 K).[9] On the other hand, thermopower after 1- mM reactions was progressively increased as a function of reaction time, but decreased with reaction times longer than 30 min. The increase of thermopower yielded a large enhancement in the power factor up to 200 %, as shown in Figure 2-2(c). These results

indicate that it is better to use low ion concentrations so as to maintain the size of particles small. Smaller particles have more surface areas for given volumes and are likely to provide more sites for charge interactions without forming a thick continuous metal layers.

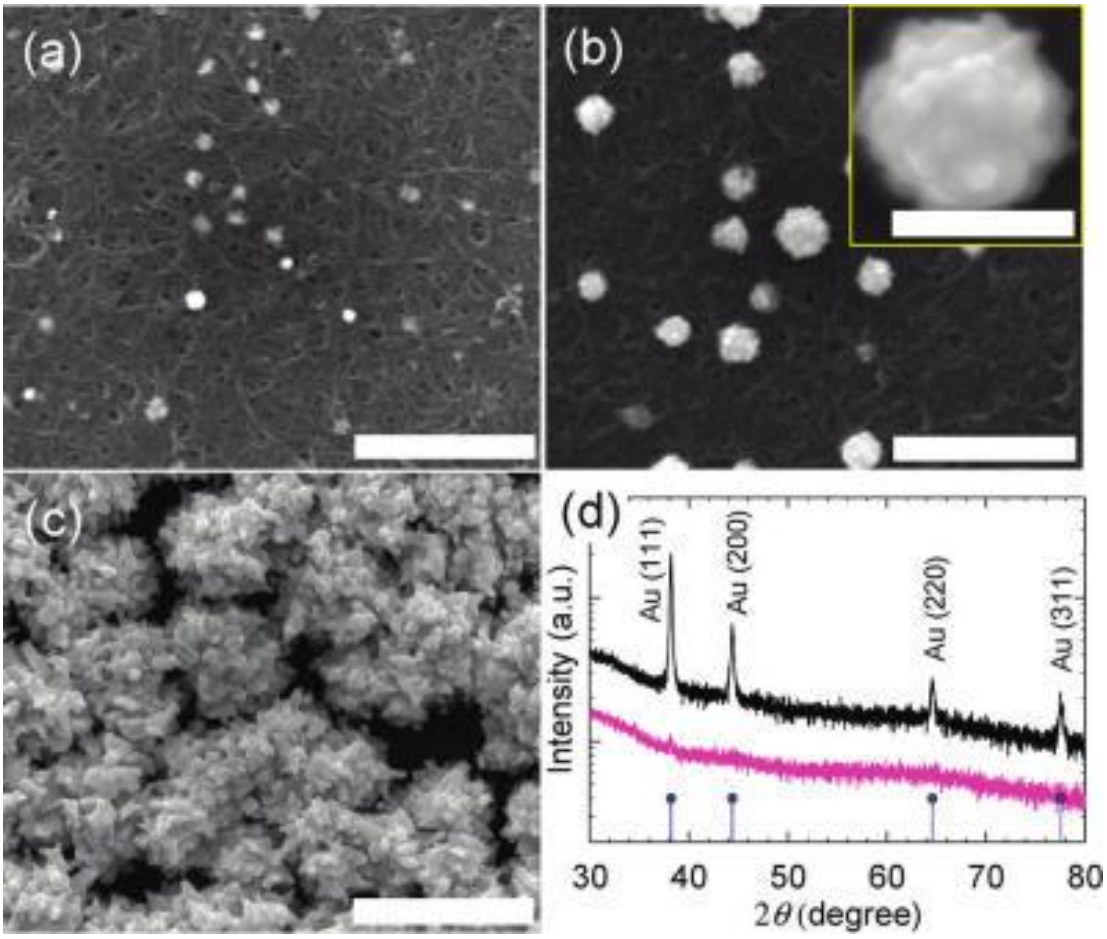

Figure 2-4 Nanotube films reacted in 1-mM $HAuCl_4$ solutions for (a) 30 sec, (b) 15 min, and (c) 120 min. The scale bars represent 2 μm and the inset scale bar 500 nm. (d) X-ray diffractions of the samples shown in (a) (lower pink line) and (c) (upper black line). Gold nanoparticles precipitated on the sites that particles were created, forming bigger particles when reaction time was increased.

In order to study transport behaviors upon changing materials, gold nanoparticles were incorporated on nanotubes as shown in Figure 2-4. Nanoparticles were precipitated by immersing nanotube films in a 1-mM $HAuCl_4$ solution for 30 sec (Figure 2-4(a)), 15 min (Figure 2-4(b)), and 120 min (Figure 2-4(c)). The large particles are composed of small ones, which indicate that the size of individual particles is a few tens of nanometers or less. Gold particles were synthesized by spontaneous gold reduction as well as galvanic displacement of silver electrodes deposited on nanotube films. The galvanic displacement was observed to be stronger than the spontaneous reduction. Without silver electrodes, gold reduction was slow, leaving only small density of nanoparticles on samples. We noticed that gold reduction could be facilitated when samples were made of nitric acid treated nanotubes (reflux in 70% HNO_3 for several hours). Presumably, functionalized and/or defective nanotube surfaces created by the acid treatment are helpful in the reduction processes. Note that samples in this study were made of purified-grade nanotubes without additional treatments and nanotubes contain 4-7 % metal (Ni, Y) impurities according to manufacturer's product information. The X-ray diffraction from a 120-min reaction (upper plot, black line in Figure 2-4(d)) clearly indicates the presence of crystalline gold, but the weak peaks from a 30-sec reaction (lower plot, pink line in Figure 2-4(d)) might be due to the small density, size, and/or amorphous structures of the particles.

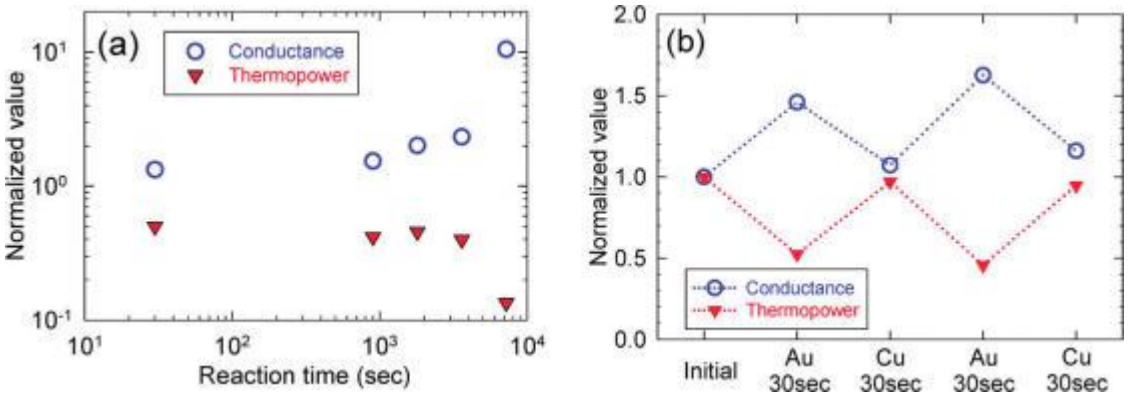

Figure 2-5 (a) Normalized conductance (blue circles) and thermopower (red triangles) as a function of reaction time after reactions in 1-mM $HAuCl_4$ solutions. (b) Normalized conductance (blue circles) and thermopower (red triangles) after two successive 30-sec reactions in a 1-mM $HAuCl_4$ solution followed by a 1-mM $CuSO_4$ solution.

The gold incorporation increased conductance of all samples with reductions in thermopower (see Figure 2-5(a)). With a long reaction (120 min) in a 1-mM $HAuCl_4$ solution, the conductance was boosted by one order of magnitude. This large increase is likely to be from electrically conducting paths along dense gold particles shown in Figure 2-4(c). Conductance and thermopower were measured when nanotube films were immersed in two different solutions (a 1-mM $HAuCl_4$ solution followed by a 1-mM $CuSO_4$ solution for 30 sec each) in series. Figure 2-5(b) indicates the changes in electrical conductance and thermopower were reversible when gold and copper were serially incorporated on nanotubes. Upon the gold incorporation, conductance was increased with a reduction of thermopower, and the copper incorporation resulted in the opposite behaviors.

The reversible change in electronic transport properties occurs when electrons are readily transferred from metals to nanotubes or vice versa depending on the work

function of metals relative to those of nanotubes. When metals are precipitated, the difference between their Fermi levels at metal-nanotube contacts induces electron transfer to equilibrate the Fermi levels. The work functions of copper, gold, and nanotubes are respectively 4.38~4.65 eV,[34,35] 5.0~5.22 eV,[35] and 4.7~5.0 eV.[28,29] Hence, when copper is in contact with nanotubes, electrons are donated to nanotubes, making them more n-type materials. On the other hand, gold incorporation makes nanotubes more p-type by withdrawing electrons from nanotubes. When gold particles are spontaneously precipitated, electrons are transferred from nanotubes to gold ions. Nanotubes have shallow density of states near the Fermi level, and small changes in carrier density are likely to alter the Fermi level of nanotubes significantly. The shift of the Fermi level may give rise to a large change in thermopower with small changes in electrical conductivity. When the Fermi level is located near the spike in the density of states of nanotubes, such changes of thermopower would result in a net increase of the power factor such as the case of the 1 mM-30 min copper reaction shown in Figure 2-3(c). Let's recall electrical conductivity (σ) and thermopower (S):[36]

$$\sigma = \int \psi(E)dE; \;\; \psi(E) \sim D(E)(-\partial f_{FD} / \partial E) \tag{1}$$

$$S = -\frac{1}{eT}\frac{\int \psi(E)(E - E_f)dE}{\int \psi(E)dE}; \;\; |S| \sim \frac{|E_m - E_f|}{eT} \equiv \frac{\Delta}{eT} \tag{2}$$

Here, E and E_f stand for energy and the Fermi level. $D(E)$ and f_{FD} are the electronic density of states and the Fermi-Dirac distribution. e and T are electron charge and temperature. Δ is the energy gap between mean energy (E_m) of the differential electrical conductivity ($\psi(E)$) and the Fermi level, E_f. Electrical conductivity can be represented by

the area under the differential electrical conductivity since it is obtained by integrating $\psi(E)$ from the definition in Eq. (1). In order to obtain a large thermopower, it is necessary to increase Δ (see Eq. (2)), which can be obtained by making the shape of $\psi(E)$ anisotropic.

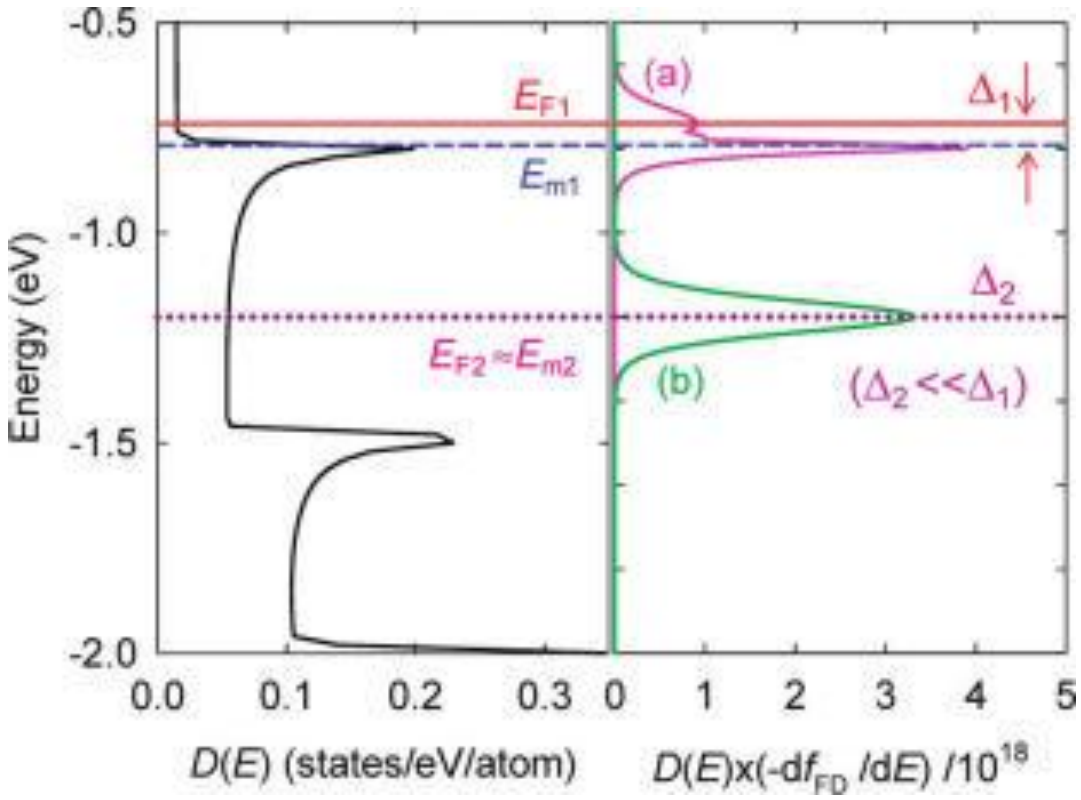

Figure 2-6 (Left pane) Electronic density of states ($D(E)$) for a single wall carbon nanotube with (10,10) chirality. (Right pane) Energy against $D(E)(-\partial f_{FD}/\partial E)$ that is proportional to the differential electrical conductivity (ψ in Eq.(1)). (a) $D(E)(-\partial f_{FD}/\partial E)$ when the Fermi level, E_{F1} is near the spike-shape density of states (pink line). The gap (Δ_1) between E_{F1} and E_{m1} is relatively large, increasing the magnitude of thermopower ($|S|$). (b) $D(E)(-\partial f_{FD}/\partial E)$ when the Fermi level, E_{F2} is near the flat density of states (green line). The gap (Δ_2) between E_{F2} and E_{m2} is very small, leading to small thermopower.

This behavior is conceptually described in Figure 2-6 with a metallic nanotube of (10,10) chirality. The density of states (black solid line in Figure 2-6 left pane) was calculated by the local density approximation of density functional theory.[37] When electrons are injected 'to' nanotubes by copper incorporation, the Fermi level is located at an energy level higher than that of nanotubes decorated by gold (electrons are withdrawn 'from' nanotubes). For example, the red solid (E_{F1}) and purple dotted (E_{F2}) lines may represent the Fermi levels after copper and gold reactions, respectively. Figure 2-6(a) and (b) (Figure 2-6 right pane) represent $D(E)(-\partial f_{FD}/\partial E)$, which is proportional to the differential electrical conductivity (ψ in Eq.(1)), for the samples after (a) copper and (b) gold reactions, respectively. When the Fermi level of nanotubes is located near the energy level where the density of states is spike-like shape (e.g., E_{F1}), the differential electrical conductivity becomes anisotropic (see the pink solid line (a) in Figure 2-6). This enlarges the energy gap, Δ_1 ($\equiv |E_{m1} - E_{F1}|$) that is proportional to the magnitude of thermopower. When n-doping is so strong that the Fermi level is raised well above E_{F1} towards the flat regime, the differential electrical conductivity becomes symmetric, decreasing the magnitude of thermopower. This behavior was observed when reaction time is longer than 1 mM-30 min as shown in Figure 2-3(b). Note that this is not likely from the small thermopower of copper because conductance was monotonically decreased with increasing reaction time. In other words, the 1-mM concentration is too low to form continuous copper films within the time period of our experiments, resulting in a monotonic reduction of hole concentrations in nanotubes. If copper nanoparticles were connected each other, conductance would have been considerably increased like

the 20 mM-30 min experiment (see blue squares in Figure 2-3(a)). On the contrary, when nanotubes become more p-type and the Fermi level is located near a flat regime of the density of states, the shape of the differential electrical conductivity is symmetric, resulting in small Δ_2 ($\equiv |E_{m2} - E_{F2}|$) (see the green solid line (b) in Figure 2-6). When nanotubes were additionally doped with oxygen by annealing samples in a tube furnace at 250 ℃ with 10 sccm oxygen flow for 3 hours, thermopower was further increased. This is likely from additional p-type doping that lowers the Fermi level close to another spike in the density of states. Upon vacuum annealing at ~10^{-8} Torr at 250 ℃ for 3 hours, thermopower was decreased likely due to oxygen desorption.

2.4. Conclusion

In summary, nanoparticle incorporation on nanotubes modulated electrical conductance and thermopower of nanotube films, raising their thermoelectric power factors. Nanotubes were made into films by spraying nanotube solutions on glass substrates. Then, copper or gold ions were reduced by immersing the films into $CuSO_4$ or $HAuCl_4$ solution of different concentrations for various time periods. Copper was precipitated by using zinc electrodes whose reduction potential is lower than that of copper. Gold reduction was facilitated by silver counter electrodes, but at the same time gold was also spontaneously reduced on nanotubes due to the larger reduction potential of gold than those of nanotubes. Reactions in low ion-concentration solutions generated small (a few tens of nm) particles while particles coalesced during ion reduction in high concentration solutions. In case of copper incorporation, electrons were believed to be

donated to nanotubes (more n-type). Gold reduction takes electrons from nanotubes, making samples more p-type. A series of experiments at different ion concentrations and reaction time periods were systematically performed in order to reveal nanoparticle formation conditions and electronic transport changes that improve the thermoelectric power factor. The experimental results show the transport properties can be considerably altered and modulated, resulting in twofold improvement in the thermoelectric power factor with a 1 mM-30 min reaction. Reactions in low ion-concentration solutions yielded well-distributed small particles, which provided large surface areas and thereby strongly affected electrical properties of nanotubes. It has also been found that electrical property changes are reversible. Successive copper and gold decorations on nanotubes made electrical conductance (or thermopower) serially decreased and increased (or increased and decreased). These transport behaviors are believed to be from the modification of the Fermi level as a result of electron exchanges between reduced metals and nanotubes. Upon nanoparticle precipitation, electron transfer occurs in order to equilibrate the Fermi levels of materials in contact. Additionally, tube-tube junctions may have been modified as a result of bridging nanotubes with nanoparticles. The thermopower enhancement after copper decoration can be attributed to the enlarged gap between the Fermi level and the mean of differential electrical conductivity. Such behaviors often appear when the Fermi level is shifted towards the spike-shape density of states in nanotubes due to anisotropic differential electrical conductivity. Electrical conductance was improved when carrier concentrations were raised as a result of nanoparticle precipitation.

3. STUDY 2: HIGH ELECTRICAL CONDUCTIVITY AND N-TYPE THERMOPOWER FROM DOUBLE-/SINGLE-WALL CARBON NANOTUBES BY MANIPULATING CHARGE INTERACTIONS BETWEEN NANOTUBES AND ORGANIC/INORGANIC NANOMATERIALS*

Single and double walled carbon nanotubes were utilized to decorate several organic/inorganic nanomaterials. A spraying method was employed to prepare nanotube thin films as presented in study 1 and various nanomaterials were decorated on the film surface. When charge interations between nanotubes and nanomaterials are properly manipulated, p-type or n-type doping can be maximized so that high electrical conductivity or n-type thermopower is obtained. This is believed to lead to apply carbon nanotubes as p or n-type conductors which are essential to thermoelectric energy conversion application.

3.1. Background information

In this study, organic or inorganic nanomaterials were incorporated on carbon nanotubes to control carrier concentrations, which shifts their Fermi energy that yields high electrical conductivity or n-type thermopower (or the Seebeck coefficient) that are very different from those of pristine nanotubes. When double-wall carbon nanotubes

* Reprinted with permission from "High electrical conductivity and n-type thermopower from double-/single-wall carbon nanotubes by manipulating charge interactions between nanotubes and organic/inorganic nanomaterials" by Yeontack Ryu, Dallas Freeman, Choongho Yu, 2011. *Carbon*, 49(14), 4745-4751, Copyright [2011] by Elsevier Ltd.

(DWCNTs) were decorated with tetrafluoro-tetracyanoquinodimethane (F_4TCNQ), their electrical conductivities were increased up to 5.9×10^5 S/m (at least 300% improvement compared to those of air-exposed tubes) due to increased hole concentrations. Carbon nanotubes are p-type due to doping of oxygen in air[30] unless they are stored in controlled environment (e.g., vacuum or inert gas). Single-wall carbon nanotubes (SWCNTs) were converted to n-type by using polyethyleneimine (PEI) without vacuum or controlled environment with a large thermopower, -58 μV/K, whose absolute value is greater than typical thermopower (10~40 μV/K[4,11,38] from p-type single-wall nanotubes). Inorganic nanoparticles such as Cu, Fe, or Au were also decorated on both SWCNTs and DWCNTs. Fe and Cu decoration decreased electrical conductance with enlarged thermopower whereas Au decoration made nanotubes more p-type, yielding higher electrical conductance with lower thermopower. The power factors were improved by ~180% with F_4TCNQ on DWCNTs and ~140% with Fe on SWCNTs. The difference of work functions and reduction potentials between nanomaterials and nanotubes was a crucial factor to determine charge interaction to alter electrical conductivity and thermopower. The following describe experimental details, transport properties and morphologies of samples, and discussion.

3.2. Experimental procedure

3.2.1. Incorporation of F_4TCNQ and tetracyanoquinodimethane (TCNQ) molecules and Fe, Cu, and Au nanoparticles into nanotubes

12-mg of double-wall carbon nanotubes (XBC, Continental Carbon Nanotechnology) or 12-mg single-wall carbon nanotubes (P2-SWCNT, Carbon Solution company) were dispersed in DI water of 20 mL with the aid of 24-mg sodium dodecyl benzene sulfonate (SDBS) as a surfactant by ~10 min ultra-sonication. The solution was then centrifuged at 8000 rpm for 15 min to obtain a supernatant. According to the product information of P2-SWCNT, metal contents (Ni, Y) range from 4 to 7 wt % and carbonaceous purity is greater than 90 %. Average diameters of individual tubes and bundles are 1.5 and 4-5 nm, respectively. The average length of bundles ranges from 500 nm to 1.5 μm. A spray gun (GP-S1, Fuso Seiki Co.) was used to spray the as-prepared solution on a glass substrate at 80~85 ℃. The films were immersed into DI water for 30 min in order to remove the SDBS surfactant and dried by compressed air, and then baked at 60 ℃ in a vacuum oven for 2 hours.

Carbon nanotube films were immersed in F_4TCNQ or TCNQ solutions of 0.1, 1, 5, or 10 mM concentrations in dimethyl sulfoxide (DMSO) for 5 min. For the metal nanoparticle incorporation, aqueous $CuSO_4$, $FeCl_2$, or $HAuCl_4$ solutions were used. For Au decoration, the as-synthesized nanotube films were immersed into a $HAuCl_4$ solution with only silver paint electrode (spontaneous reduction). On the other hand, a galvanic displacement method was employed with Mg electrodes attached on nanotube films. Mg was dissolved in aqueous $CuSO_4$ or $FeCl_2$ solutions to precipitate Cu or Fe nanoparticles.

All films after incorporation were gently cleaned by DI water and dried by compressed air.

3.2.2. Incorporation of PEI into nanotubes

20-mg of single-walled carbon nanotubes (>90% in purity, Cheaptubes, Inc.) were dispersed by ultra-sonication for 20 min in a solution containing 4.72-g of PEI in 20 ml DMF (20 wt% PEI in the mixture solution). According to the product information, the inner and outer diameters of the nanotubes are 0.8~1.6 nm and 1~2 nm, respectively. The average length of the nanotubes ranges from 5 μm to 30 μm. The solution was stirred at a constant temperature of 50 ℃ for 2, 3, or 4 days, and then was vacuum-filtrated to remove excessive PEI and impurities by methanol and subsequently water. The PEI-incorporated nanotubes were collected and re-dispersed in DI water by using SDBS. The solution was sprayed on a glass substrate to fabricate films followed by the SDBS removal and baking processes, as mentioned above. The film thicknesses were varied from 50 nm to 600 nm.

3.2.3. Electrical measurement and characterization

A homemade four-probe setup with T-type thermocouples and two copper wires as well as two thermoelectric modules for creating temperature differences were used in electrical conductance and thermopower measurements at room temperature. Four silver line-shape electrodes were painted on both edges of nanotube films. In order to obtain film conductance, current (I) and voltage (V) were plotted by using a I-V sweeping

method across the long edge of the films. Voltages between two electrodes at both ends of the films were measured at six different temperature differences between 0 and ±7 ℃ to extract thermopower. The transport properties were measured before and after the nanomaterial incorporation and the film thickness was characterized by an optical surface profilometer (Wyko NT9100 optical profiler, Veeco Instruments Inc.). The surface morphology of the metal-decorated carbon nanotube films was inspected by using a field-emission scanning electron microscope (FEI Quanta 600) equipped with energy dispersive spectroscopy.

3.3. Results and discussion

Table 3-1 Work functions and electron affinities of carbon nanotubes and nanomaterials.

	Work function	Electron affinity (eV)
DWCNT[39,40]	4.5~5.24	-
SWCNT[14,41-43]	3.8~5.1	-
F_4TCNQ[44]	-	3.38
TCNQ[44]	-	2.8
Cu[34,35]	4.38~4.65	-
Fe[35]	4.35~4.8	-
Au[35]	4.9~5.22	-

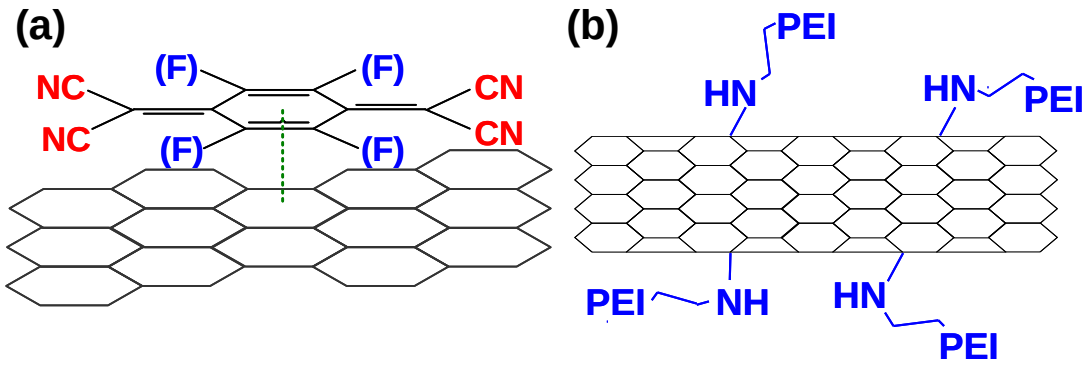

Figure 3-1 F4TCNQ or TCNQ on carbon nanotube surface forming π stacking. Fluorine (F) is present only in F4TCNQ (a); SWCNT-PEI conjugates formed by a physical absorption of PEI (b) The hexagon arrays represent nanotubes.

Several organic and inorganic nanomaterials were selected, and their work functions and electron affinities are listed in Table 3-1. F_4TCNQ[45-47] and TCNQ[48,49] have recently been studied as p-type dopants for carbon nanotubes and graphene due to their large electron affinity. These molecules are attached on nanotube surfaces by π-π stacking as shown in Figure 3-1(a). The work functions of carbon nanotubes and graphene are enlarged by the molecules due to electron transfer from carbon nanotubes to the molecules, increasing hole concentrations. On the other hand, PEI donates electrons to nanotubes, which makes it possible to convert p-type nanotubes into n-type. PEI decoration on the surface of nanotubes was thermally activated, resulting in amine-nanotube conjugates directly formed by a physical absorption as shown in Figure 3-1(b).[50,51] Recent studies[7,52] reported an n-type field effect transistor (FET) characteristic and air stability of PEI-incorporated nanotubes, but systematic studies regarding electron transport properties (e.g., electrical conductivity and thermopower) have not been reported yet. This paper also presents nanotubes with inorganic Au, Cu, and Fe

nanoparticles can be incorporated due to the differences of reduction potentials between nanotubes and metal ions (spontaneous reduction[26]) or between metals (e.g. Zn or Mg) attached to nanotubes and metal ions (galvanic displacement[25]). Both decoration mechanisms are drawn in Figure 2-1 schematically. In the galvanic displacement (Figure 2-1(a)), Mg electrodes give up electrons (e^-) to nanotubes, reducing metal ions (Mn^+) into metal nanoparticles (M^0). Spontaneous reduction (Figure 2-1(b)) provides metal ions with electrons withdrawn from nanotubes, precipitating nanoparticles on the surface of nanotubes. We have previously demonstrated it is feasible to manipulate S and σ of SWCNTs with Cu and Au nanoparticles, resulting in a net increase of the power factor.[11] Here, DWCNTs in addition to SWCNTs were tested with three different nanoparticles (Fe, Cu, Au) to compare their influence on transport properties. The following describe experimental procedures as well as electrical properties of nanotubes upon decorations of different molecules and nanoparticles.

In order to prepare samples with F_4TCNQ, TCNQ, and nanoparticles (Fe, Cu, Au), carbon nanotubes were dispersed in deionized (DI) water with the aid of sodium dodecyl benzene sulfonate (SDBS) as a surfactant. The nanotube solution was centrifuged and then supernatant was sprayed on a glass substrate. As-prepared carbon nanotube films were immersed into solutions containing the molecules or the metal ions. PEI-decorated nanotubes were prepared separately because PEI is not soluble in water. First, PEI was dissolved in dimethyl formamide (DMF), and then nanotubes were dispersed in the solution. After stirring and subsequent filtration processes, nanotubes were re-dispersed in water with SDBS and sprayed on a substrate. Electrical resistances

and thermopowers of as-prepared samples were measured and the power factors were calculated. Electrical conductivities and thermopowers of DWCNT films were measured to be ~2×10^5 S/m and 55~65 μV/K, respectively. The film thicknesses were measured to be 50~70 nm. The high conductivity can be attributed to high concentration of metallic tubes (no band gaps due to relatively large tube diameters) or the presence of π conducting channels formed between inner and outer walls.[53]

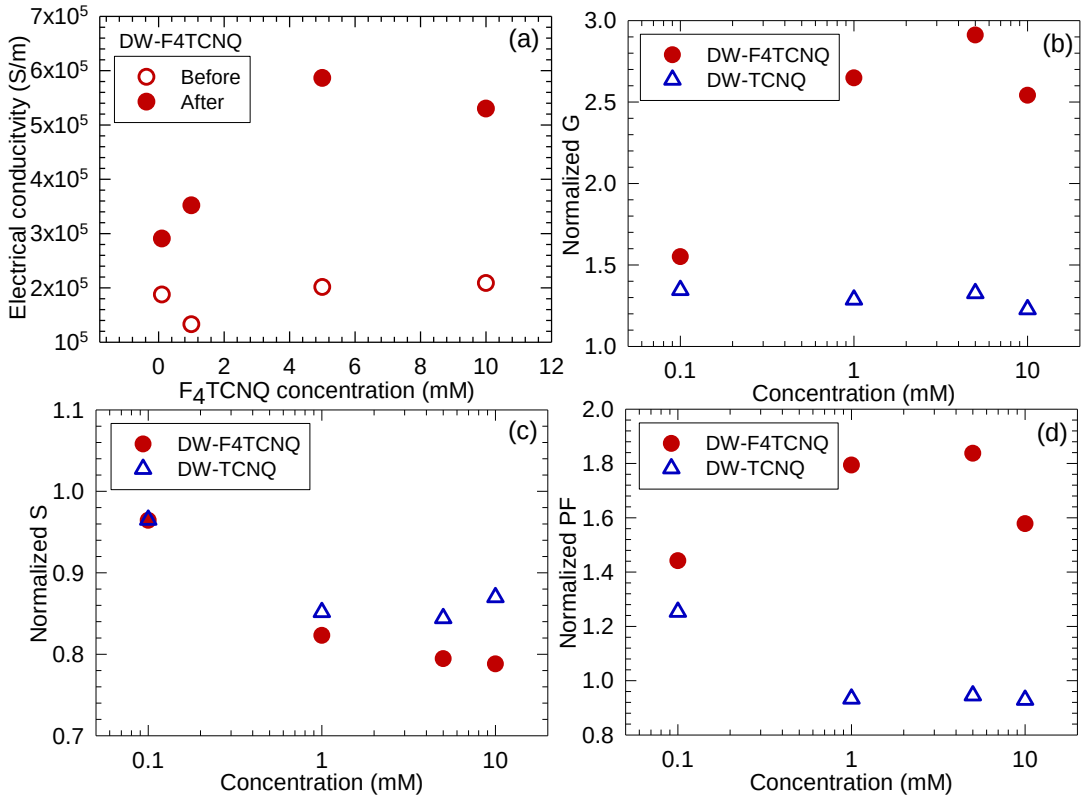

Figure 3-2 Electrical conductivities of DWCNT films (DW) before and after F4TCNQ incorporation (a) Normalized conductance, G (b), thermopower, S (c), and the power factor, PF (d) after 5 min reactions in a F4TCNQ or TCNQ solution as a function of concentration.

When the as-prepared samples were immersed for 5 minutes in dimethyl sulfoxide (DMSO) with F_4TCNQ or TCNQ of 0.1, 1, 5, and 10 mM concentrations, the electrical conductivity was increased up to ~5.9×10^5 S/m with 5 mM F_4TCNQ (Figure 3-2(a)). This conductivity is three times higher than those of the pristine DWCNT films (see the normalized conductance in Figure 3-2(b)) and orders of magnitude higher than typical nanotube films.[54-56] On the other hand, 0.1~10 mM TCNQ slightly improved the conductance with a weak concentration dependence (Figure 3-2(b)). It should be noted that the 'normalized' conductance, thermopower, and the power factor respectively indicate those divided by the properties prior to molecule/nanoparticle incorporations. The increases in conductance were accompanied by up to 20% reduction in the thermopower for both F_4TCNQ and TCNQ (Figure 3-2(c)), which resulted in a net increase of the power factor by a factor of 1.8 (Figure 3-2(d)). The maximum power factor with TCNQ was obtained at 0.1 mM concentration, yielding a normalized power factor of 1.3 (Figure 3-2(d)). The maximum electrical conductivity of the TCNQ-incorporated film was measured to be ~2.3×10^5 S/m at the same concentration, which is lower than that of the F_4TCNQ-incorporated films. This is likely to be from the larger work function difference between DWCNT and F_4TCNQ than that between DWCNT and TCNQ (see Table 3-1). When molecules of a work function larger than that of nanotubes are made a contact with nanotubes, electrons are often transferred from the nanotubes to molecules to equilibrate the energy level. The larger the difference of the work functions is, the more electrons transfer occurs. This charge transfer increases hole concentrations in the nanotubes and also shifts the Fermi level toward the highest

occupied molecular orbital (HOMO).[11] Reactions with higher F_4TCNQ and TCNQ concentrations saturated σ and S, suggesting that there may be no more sites in the nanotubes for further incorporations. The property change is strongly dependent on the interaction between the molecules and nanotubes, not the electrical properties of the molecules. Otherwise, the properties would have continuously changed upon reactions with higher concentration solutions. However, it may be possible to increase the conductivity more than a factor of three, considering a large portion of unexposed nanotube surfaces due to the difficulty in separating nanotubes individually even with a surfactant. For instance, the diameter of typical nanotube bundles is in the range of 10 nm or less, which makes it possible to estimate the number of nanotubes in one bundle to be at least 20 nanotubes.

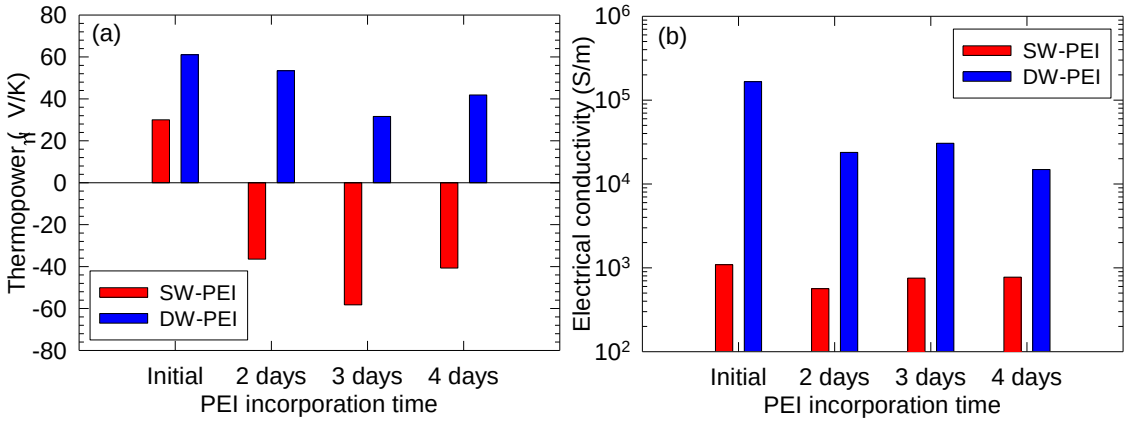

Figure 3-3 Thermopower (a) and electrical conductivity (b) of SWCNTs (SW) and DWCNTs (DW) before and after PEI incorporation for 2, 3, and 4 days.

Unlike the p-type dopants, electron-donating amine groups can provide electrons to nanotubes.[57] This moves the Fermi level of nanotubes toward the lowest

unoccupied molecular orbital (LUMO). For SWCNTs, this resulted in negative thermopowers, which indicate nanotubes have n-type characteristics. However, the thermopower of DWCNTs was not changed to a negative value (Figure 3-3(a)). Large hole concentrations in DWCNTs may have it difficult to convert them to an n-type material. Furthermore, the influence of PEI decorations may not be as strong as the case for SWCNTs because PEI cannot be incorporated on the inner tubes of DWCNTs. This may suggest the length that affected by PEI is relatively shorter than other nanomaterials studied in this paper. After a long PEI incorporation processes for 2 and 3 days, thermopowers of DWCNTs were decreased because thermopower from holes were likely to be cancelled by electrons. It should be noted that the mixture solution of PEI was stirred for days before the spraying process in order to maximize PEI concentrations on nanotubes. Thermopower seems to be saturated after three days of incorporation (Figure 3-3(a)), which may be due to fully incorporated PEI on the available surfaces of nanotubes. The n-type was maintained for at least several days, indicating the n-type conversion is irreversible in air. Electrical conductivities were also measured and compared before and after the incorporation in Figure 3-3(b), and were decreased by factors of 0.5 and 0.1 for SWCNT and DWCNT, respectively. Further changes in S and σ are very likely to happen if nanotubes are fully separated, considering only a fraction of nanotube surfaces are exposed to PEI and relatively short lengths affected by PEI.

Inorganic nanoparticles were precipitated on as-prepared DWCNT films by immersing them in $FeCl_2$, $CuSO_4$, and $HAuCl_4$ solutions of 0.01, 0.1, 0.5, 1, 2.5, 5, 7.5, 10, or 20 mM concentration. SWCNT films were also immersed in $FeCl_2$ solutions for

comparison. Reactions with higher metal ion concentrations resulted in more and bigger nanoparticles as well as larger change in conductance and thermopower as shown in Figure 3-4.

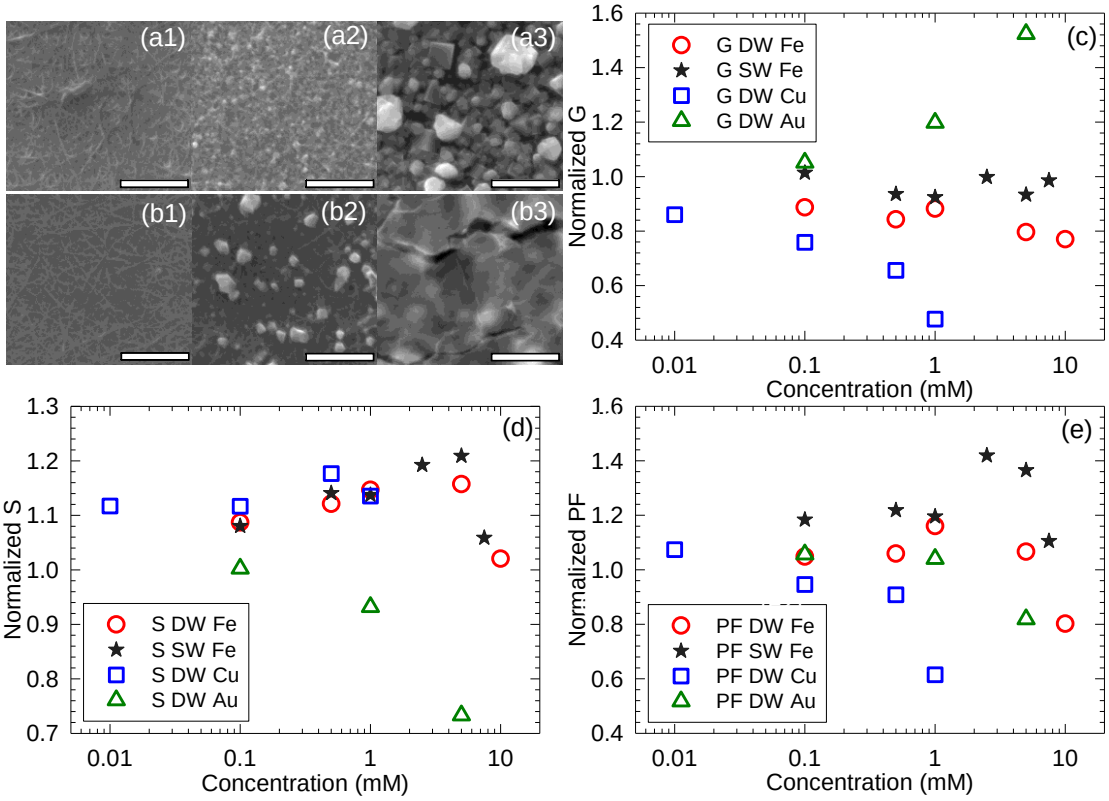

Figure 3-4 DWCNT films after 5 min reaction in $CuSO_4$ and $FeCl_2$ solutions with the following concentrations: (a1) 0.01 mM/Cu, (a2) 1 mM/Cu, (a3) 5 mM/Cu, (b1) 0.1 mM/Fe, (b2) 1 mM/Fe, (b3) 20 mM/Fe. All scale bars represent 1 micron. Normalized conductance, G (c), thermopower, S (d), and the power factor, PF (e) after 5 min reaction in $FeCl_2$, $CuSO_4$, and $HAuCl_4$ solutions as a function of ion concentrations.

For Fe or Cu decorated nanotubes, conductance (Figure 3-4(c)) decreases with increasing thermopower (Figure 3-4(d)) as a function of metal ion concentration for both DWCNT and SWCNT films, whereas Au decorated films show the opposite trend. This

is because Cu and Fe have smaller work functions and Au has a larger work function than that of carbon nanotubes. In other words, Cu and Fe donate electrons to nanotubes, decreasing hole concentrations in nanotubes while Au acquires electrons from nanotubes, raising hole concentrations in nanotubes. Cu and Fe have similar work functions (Table 3-1) and the reduction potential differences between Mg ($Mg^{2+} + 2e^- \rightarrow Mg(s)$, $E^0 = -2.372$ V)[1] and Cu ($Cu^{2+} + 2e^- \rightarrow Cu(s)$, $E^0 = +0.34$ V)[11] as well as Mg and Fe ($Fe^{2+} + 2e^- \rightarrow Fe(s)$, $E^0 = -0.44$ V)[11] are similar. Note that Mg electrodes were used for Cu or Fe reduction (galvanic displacement). Nevertheless, Cu nanoparticles (Figure 3-4(a2)) are much smaller than Fe (Figure 3-4(b2)). It appears that Fe nucleation was preferentially occurred on the site where nanoparticles initially formed, generating sparsely distributed large particles. Cu particles, on the other hand, were small and uniformly distributed, which is likely to have more charge interactions between the particles and nanotubes. We believe this have caused larger conductance changes with Cu particles than Fe (i.e., compare red hollow circles for Fe and blue squares for Cu in Fig 4c). Thermopower was suddenly decreased after a Fe reduction at 10 mM (Figure 3-4(d)). This is believed to be from layers of Fe whose thermopower (15 μV/K at 300 K)[9] is smaller than nanotubes. After reactions with higher Cu and Fe concentrations (20 mM for Fe and 5 mM for Cu), sudden conductance increases up to ~400 % were observed (not shown in Figure 3-4). Such large increases would be due to electrically connected Cu and Fe nanoparticles on the nanotube surface as confirmed in Figure 3-4(a3) and (b3). The power factor, $S^2\sigma$was calculated and plotted in Figure 3-4(e), showing improvement by factors of ~1.2 (1 mM/Fe-DWCNT) or ~1.4 (2.5 mM/Fe-SWCNT).

3.4. Conclusion

Electrical transport properties of carbon nanotube films were altered by incorporating organic or inorganic nanomaterials. F_4TCNQ, TCNQ, Cu, Fe, and Au nanomaterials were decorated on nanotube films that were fabricated by a spraying method, whereas PEI was incorporated into nanotubes by a stirring process and then PEI-nanotube bundles were made into films. Electrical conductance and thermopower of nanotube films before and after nanomaterial decorations were measured to evaluate their influence on thermoelectric transport properties including electrical conductivity and thermopower. F_4TCNQ or TCNQ decoration made the carbon nanotube film more p-type by extracting electrons from nanotubes. In particular, F_4TCNQ-incorporated DWCNTs generated 300 % improvement in conductance, yielding very high electrical conductivities up to ~5.9 S/m. On the other hand, PEI decoration on nanotubes made p-type nanotubes (due to oxygen in air environment) converted to n-type by donating electrons to nanotubes. A large negative thermopower, -58 μV/K was obtained and maintained for at least several days. The n-type conversion was achieved only with SWCNTs, but not with DWCNTs. This selective conversion is likely to be from less available sites for PEI decoration (i.e., inner walls are not exposed) as well as a large hole concentrations in DWCNTs. Inorganic nanoparticles including Au, Fe, or Cu were also decorated on DWCNTs or SWCNTs by using a spontaneous reduction or a galvanic displacement method. Fe and Cu decoration decreased electrical conductance with enlarged thermopower due to the reduction of hole concentrations. On the other hand, Au decoration made nanotubes more p-type, yielding higher electrical conductance with

lower thermopower due to increased hole concentrations. Fe nucleation was preferentially occurred on the site where nanoparticles initially formed, generating sparsely distributed large particles. Cu particles, on the other hand, were small and uniformly distributed, causing larger changes in conductance than Fe. The power factors were improved by ~180% with F_4TCNQ on DWCNTs and ~140% with Fe on SWCNTs. The difference of work functions and reduction potentials between nanomaterials and nanotubes was a crucial factor to determine charge interaction to alter electrical conductivity and thermopower. This study shows a first step toward the synthesis of both n-type and p-type conductors with carbon nanotubes, which are essential to thermoelectric energy conversion applications.

4. STUDY 3: THE INFLUENCE OF INCORPORATING ORGANIC MOLECULES OR INORGANIC NANOPARTICLES ON THE OPTICAL AND ELECTRICAL PROPERTIES OF CARBON NANOTUBE FILMS*

Carbon nanotube thin films prepared by a spraying method can be used as transparent and conductive electrode. Square-shaped films on glass substrate are post-processed by various chemicals in order to incorporate organic/inorganic nanomaterials as well as the films are microwave-irradiated. Sheet resistance is measured before and after the surface modification by a home-made four probe measurement setup. Optical transmittance is also measured by a UV-VIS spectroscopy. It is meaningful to identify the performance of the transparent and conductive electrode made by carbon nanotubes when they are chemically or physically modified with various ways.

4.1. Background information

In this study, Au, F_4TCNQ, or $HNO_3/SOCl_2$ was used for doping both SWNTs and DWNTs. The HNO_3 treatment removes impurities used for synthesizing nanotubes and thereby reduces the resistance of nanotube networks.[58] The $HNO_3/SOCl_2$ treatment enhances the electrical properties of nanotubes because electronegative HNO_3 molecules or acyl chloride from $SOCl_2$ provide holes to nanotubes. The HNO_3 molecules are

* Reprinted with permission from "The influence of incorporating organic molecules or inorganic nanoparticles on the optical and electrical properties of carbon nanotube films" by Yeontack Ryu, Choongho Yu, 2011. *Solid State Communications*, 151, 1932-1935, Copyright [2011] by Elsevier Ltd.

intercalated within nanotube networks[59] and the acyl chloride is substituted for carboxyl acid groups on nanotube.[41,60,61] It was reported that Au nanoparticle decoration on nanotube films also gives rise to p-type doping effects with negligible changes in optical transparency.[14,40] Particularly F_4TCNQ has been known as a hole doping material due to its higher electron affinity,[45,47] but it has been barely studied for the applications utilizing transparent and conductive properties.

We also employed microwave irradiation that is believed to remove metallic catalysts or impurities[62] and metallic nanotubes[63-65] as well as heal[66] or create[67,68] defects depending on the microwave irradiation intensity and environment. In this work, the microwave irradiation was performed under a high vacuum environment (~10^{-7} Torr) in order to increase the sites for decorating nanomaterials on the nanotube surface so as to maximize doping. Our series of experiments not only demonstrate very high electrical conductivity achieved with the DWNT films but also depict comparative studies for electrical/optical properties depending on nanotube types (SWNT and DWNT) and surface decorations/modifications (F_4TCNQ, Au, $HNO_3/SOCl_2$, and microwave irradiation).

4.2. Experimental procedure

DWNTs (XBC, Continental Carbon Nanotechnology) and SWNTs (P2-SWNT, Carbon Solution) used in the study were synthesized by using a chemical vapor deposition and an arc discharge method, respectively. According to the product information, the DWNTs samples contain double-wall tubes with inner-tube diameters

of 0.9-2.4 nm and outer-tube diameters of 1.5-3.0 nm with some single- and triple-wall tubes as impurities. The SWNT samples have metal contents (Ni, Y) range from 4 to 7 wt % and carbonaceous purity greater than 90 %. Average diameters of individual tubes and bundles are 1.5 and 4-5 nm, respectively. The average length of bundles ranges from 500 nm to 1.5 μm.

12-mg of DWNTs or 12-mg of SWNTs were dispersed in 20-mL of deionized (DI) water with an aid of 24-mg of sodium dodecylbenzene sulfonate (SDBS) in a bath-type sonicator for 30 min, and then the solution was centrifuged at 8000 rpm for 15 min. The supernatant was sprayed on soda-lime glass substrates (microscope slides) or quartz substrates (only for the microwave experiments) whose surface temperatures were maintained at 80°C during the spraying. Then, the films were immersed in deionized (DI) water for 30 min in order to remove the SDBS surfactant and dried by compressed air.

The as-prepared nanotube films were immersed in 20-mM $HAuCl_4$ in DI water for 20 min or 5-mM F_4TCNQ in 99.9 % dimethyl sulfoxide (DMSO) for 5 min. For the $HNO_3/SOCl_2$ incorporation, the as-prepared films were successively dipped into 70 % HNO_3 and then 99 % $SOCl_2$ solutions for 30 min each. After the $SOCl_2$ treatment, the films were naturally dried in air because SOCl2 molecules dissolve in water. For the microwave irradiation experiment in a vacuum environment, a chamber was located in a 900-W microwave oven. The films were placed in the vacuum chamber whose bottom was sealed with a quartz plate so that microwave can be transmitted. Microwave was irradiated on the films for total 100 sec (20 times of intermittent 5 sec operations and 5 min breaks) after the vacuum level reached ~10^{-7} Torr.

A homemade four-point probe setup was used to measure sheet resistance of square (2×2 cm^2) thin film samples at room temperature. Four dot-shape silver electrodes were painted on the four edges of the films. In order to obtain the sheet resistance of the films by using the Van der Pauw method, slopes from linear current (I)-voltage (V) plots were obtained in the horizontal or vertical direction of the films. Transmittance was measured by using a UV-Vis-NIR spectrophotometer (Hitachi U-4100). Raman spectra of the nanotubes were characterized by using Raman spectroscopy (Horiba Jobin-Yvon Lab Ram IR) apparatus.

4.3. Results and discussion

Figure 4-1(a) depicts the sheet resistance as a function of transmittance at 550 nm. In general, the DWNT films are more conductive than the SWNT films at the same transmittance. For instance, DWNT and SWNT films respectively have 124 Ω/sq and 262 Ω/sq at 76 % transmittance. The lower resistance from the DWNT films is likely to be due to their overall metallic behaviors[69] and superior conducting channels in concentric tubes. Tube-tube interactions in SWNT bundles could be a barrier in electron transport,[70] but DWNTs have π channels bewteen inner and outer tubes as well as the inner tube isolated from other tubes that may give rise to the high conductivity.[71,72]

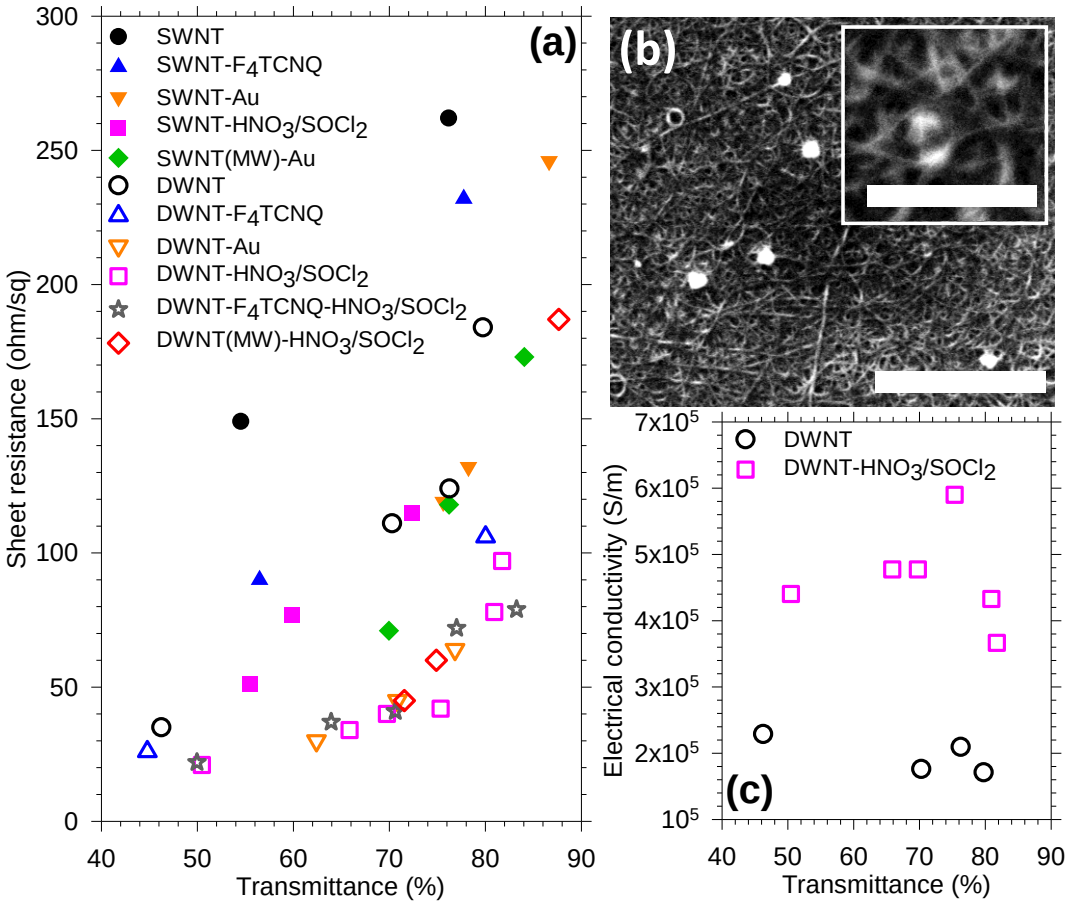

Figure 4-1 (a) Sheet resistance vs transmittance for SWNT and DWNT films when F_4TCNQ, Au, or $HNO_3/SOCl_2$ was incorporated on the pristine or microwave (MW)-irradiated nanotube films. (b) A scanning electron micrograph of a Au-incorporated DWNT film. The scale bar indicates 2 μm (500 nm for the inset). (c) Electrical conductivities of the pristine DWNT films and $HNO_3/SOCl_2$-incorporated DWNT films calculated by Eq. (3).

The incorporation of F_4TCNQ on the DWNT films made them electrically more conductive, yielding 106 Ω/sq at 80 % transmittance. F_4TCNQ is an organic molecule with a high electron affinity (~3.38 eV[44]), which moves electrons in nanotubes towards the attached molecules and thereby provides holes to the nanotubes. The incorporation of Au nanoparticles on the DWNT films showed better properties, 45 Ω/sq at 71 %

transmittance. The Au nanoparticles were decorated on the nanotube surface by spontaneous reduction[26] as shown in Figure 4-1(b). The reduction potential[1] of $AuCl_4^-$ is larger than the work function[28,29] of nanotubes, precipitating Au nanoparticles by accepting electrons from nanotubes.[11] In addition, the higher work function (4.9~5.22 eV[35]) of Au than that of nanotubes enables electrons in nanotube to move towards Au. The improvement from the Au incorporation can be attributed to a slight reduction of transmittance compared to a large increase of the electrical conductance.

The $HNO_3/SOCl_2$-incorporated DWNT films showed the similar performance with the Au-incorporated DWNT films, yielding 42 Ω/sq at 75 % transmittance. These results show the p-type doping effects by the Au and $HNO_3/SOCl_2$ incorporation are stronger than that by the F_4TCNQ incorporation. Similar trends were also observed from the experiments with the SWNT films. When the $HNO_3/SOCl_2$ treatment was used after the F_4TCNQ incorporation on DWNT films, the electrical properties were not further improved compared to those of only $HNO_3/SOCl_2$-incorporated DWNT films.

We also performed microwave irradiation on the nanotube films in order to create more defect sites for further incorporation when the microwave-irradiated SWNT and DWNT films were dipped into Au ion or $HNO_3/SOCl_2$ solutions. The irradiation under a vacuum environment minimizes a removal of nanotubes due to the lack of oxygen. We observed that the sheet resistances were slightly increased after irradiation. Nevertheless, the performances shown in Figure 4-1(a) is close to that of Au or $HNO_3/SOCl_2$ incorporated samples without microwave (see SWNT-Au vs. SWNT(MW)-Au plots as well as DWNT-$HNO_3/SOCl_2$ vs. DWNT(MW)-$HNO_3/SOCl_2$

plots in Figure 4-1(a)). We believe the microwave irradiation on carbon nanotube films has two simultaneous effects that increase and decrease the sheet resistance. The resistance increases due to a removal of nanotubes and a creation of defects. On the other hand, the defects provide opportunities of additional doping, which decrease the sheet resistance. In our experiments, the two effects are likely to have similar influence, and thereby make the sheet resistance relatively constant.

Figure 4-1(c) presents the electrical conductivities of the DWNT films and the $HNO_3/SOCl_2$-incorporated DWNT films. They were calculated by using Eq. (3), where T, Z_0, R_s, σ_{op}, and σ_{dc} are respectively transmittance, impedance of free space, sheet resistance, and optical conductivity.[73] Z_0 and σ_{op} values were taken as 377 Ω[74] and 200 S/cm,[75] respectively.

$$\sigma_{dc} = \frac{Z_0 \sigma_{op}}{2R_s}\left(\frac{1}{T^{-0.5}-1}\right) \tag{3}$$

The equation can be used when films are thinner than the wavelength of incident light for measurements and reflection is less than absorption.[76] Each sample has a different thickness within the range of 50~100 nm. The electrical conductivity of the pristine DWNT films (~2×10^5 S/m in) was significantly improved to a very high conductivity (4×10^5~6×10^5 S/m) with the $HNO_3/SOCl_2$ treatment. In the work of the reference,[76] the electrical conductivity is slightly higher than our values by using chlorosulfonic acid to de-bundle carbon nanotubes. However, the high reactivity of the chlorosulfonic acid with moisture and oxygen makes it very difficult to prepare and handle samples as well as requires thorough washing processes. We prepared our samples with a water based

solution, and then used a simple dipping process to obtain the decent electrical conductivity comparable to that of the reference.

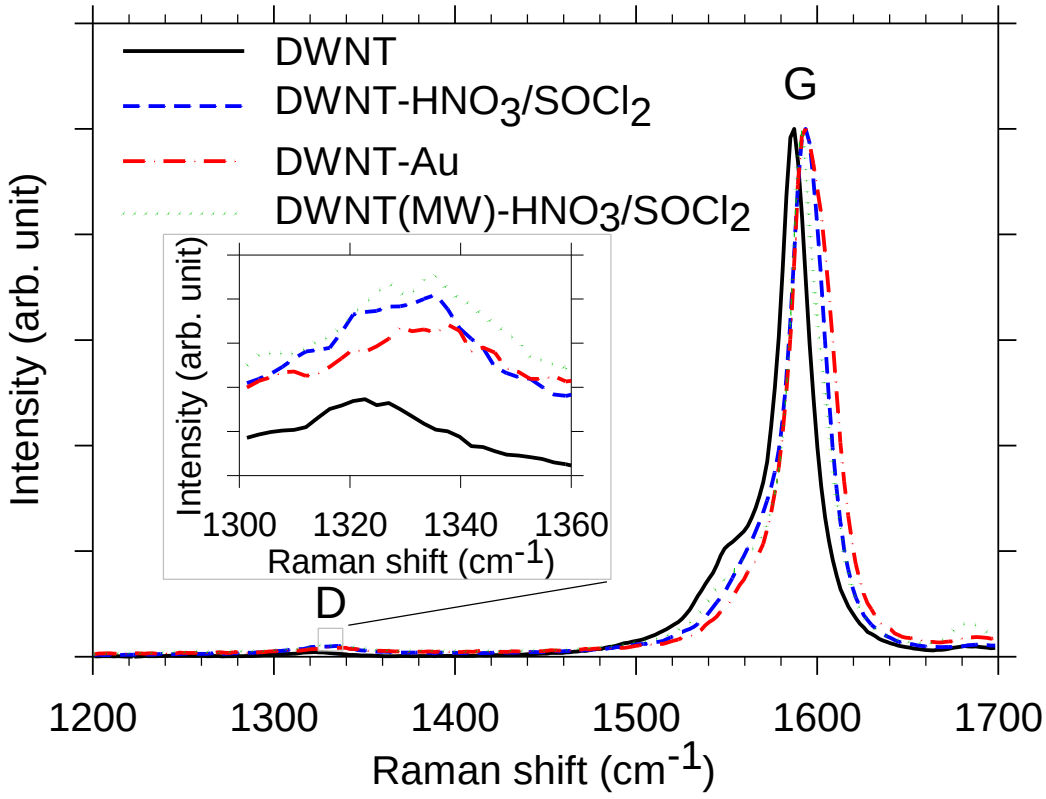

Figure 4-2 Raman spectra of a pristine (black solid line), HNO3/SOCl2-incorporated (blue broken line), Au-incorporated (red dotted-broken line), and microwave (MW)-irradiated and HNO3/SOCl2-incorporated (green dotted line) DWNT films.

The doping effects were further analyzed with the Raman spectra normalized by the G-mode intensity, as shown in Figure 4-2. The G-mode is associated with planar vibrations of carbon atoms and the D-mode represents structural defects.[77] The D-mode intensity (I_D) increased after the $HNO_3/SOCl_2$ treatment (blue broken line) compared to the pristine DWNT films (black solid line). The ratio of D-mode to G-mode (I_D/I_G) for

$HNO_3/SOCl_2$-DWNT film and DWNT film were calculated to be 0.0205 and 0.0158, respectively. This can be attributed to the HNO_3 acid treatment that creates defect sites. After the microwave irradiation, a further increase in the D-mode intensity (I_D/I_G = 0.0226) was observed indicating relatively dense defects on the nanotubes. On the other hand, the G-mode frequencies from the Au- (red dotted-broken line) or $HNO_3/SOCl_2$-incorporated (blue broken line) DWNT films were up-shifted from 1587 cm^{-1} of the pristine DWNT film (black solid line) to 1594 cm^{-1}, as shown in the Figure 4-2, indicating typical p-doping behaviors.[78]

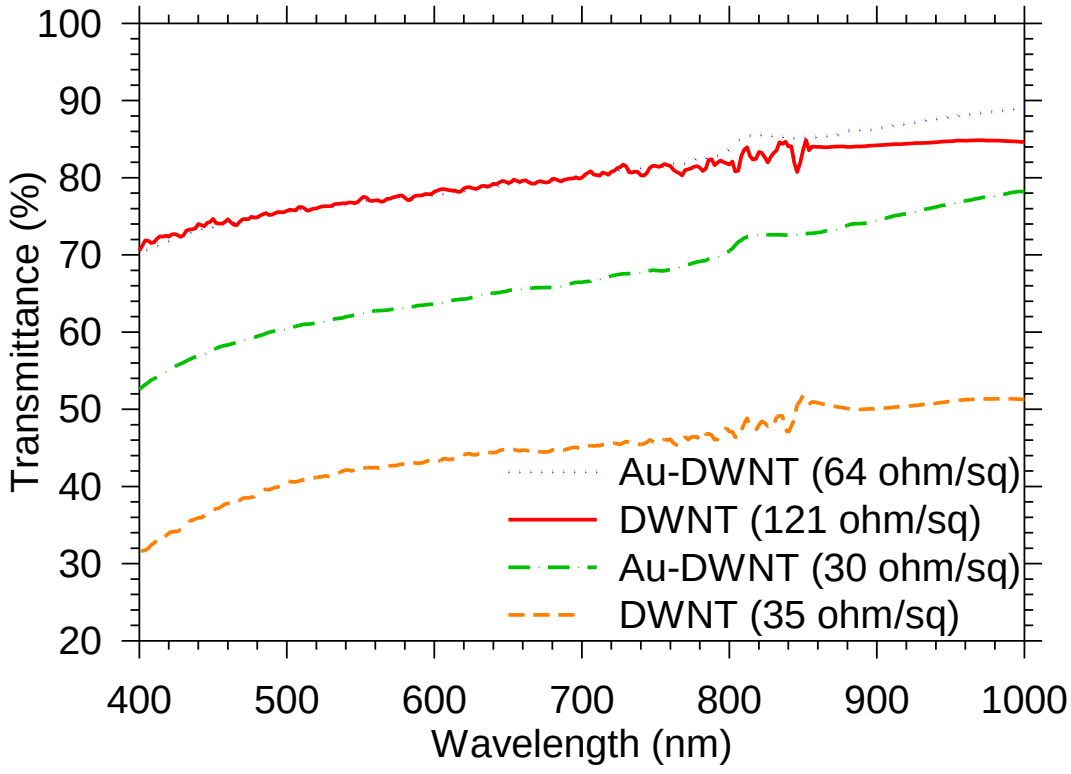

Figure 4-3 Transmittance spectra of DWNT films (121 and 35 Ω/sq) and Au-incorporated DWNT films (64 and 30 Ω/sq) as a function of incident light wavelength.

Figure 4-3 shows the transmittance spectra of two DWNT films and two Au-incorporated DWNT films. The top two plots are from the Au-DWNT film (blue dotted line) with 64 ohm/sq and the DWNT film (red solid line) with 121 ohm/sq. It should be noted that the transmittances were very similar and even higher for the Au-DWNT above ~800 nm. Two other samples have similar sheet resistances, 30 ohm/sq for the Au-DWNT film (green dotted-broken line) and 35 ohm/sq for the DWNT film (orange broken line). It is noted that spectral shapes are very similar with each other in visible range (400~800 nm) for all samples but the slopes of the Au-DWNT films are slightly steeper in near-infrared region (850~1000 nm). Additionally, the small fluctuations from the pristine DWNTs near 800 nm seem to be smoothened when Au was decorated.

4.4. Conclusion

In summary, systematic and comparative studies for electrically conductive and optically transparent p-type doped carbon nanotube films were performed. We used F_4TCNQ molecules, Au nanoparticles, and $HNO_3/SOCl_2$ molecules on both SWNT and DWNT films as p-type dopants in order to decrease sheet resistance without deteriorating transmittance. The $HNO_3/SOCl_2$ or Au was evaluated to be the strongest p-type dopants. The $HNO_3/SOCl_2$-incorporated DWNT film yielded a very high electrical conductivity, $\sim 6\times 10^5$ S/m and the sheet resistance at 75 % of transmittance was measured to be 42 Ω/sq. We also observed similar properties when Au nanoparticles were incorporated into DWNT films. The p-doping effects were also identified from the up-shift in the G-mode of the Raman spectra. More defects were observed from the

$HNO_3/SOCl_2$ incorporation and microwave irradiation experiments. The Au decoration reduced the sheet resistance without sacrificing the transmittance. We believe further studies may lead to better carbon-based transparent and conductive electrodes.

5. STUDY 4: DRAMATIC ELECTRICAL CONDUCTIVITY IMPROVEMENT OF CARBON NANOTUBE NETWORKS BY SIMULTANEOUS DE-BUNDLING AND HOLE-DOPING WITH CHLOROSULFONIC ACID*

Filtration system was employed to prepare carbon nanotube films with different dispersion method. Three representative dispersing agents and four different carbon nanotubes were mixed and twelve different nanotube films were compared and analyzed in terms of their morphology by scanning electron micrograph, transmission electron micrograph, and Raman spectroscopy. Debundling effect of a strong acid without loss in nanotube defects is verified by measuring electrical conductivity of the nanotube films. Effect of nanotube network morphology after surface modification on thermopower is also investigated. These are very important study because most industrial applications were performed by bulk carbon nanotube materials forming network.

5.1. Background information

The degree of separation (or dispersion), which can be identified by the diameter of nanotube bundles, is a strong functin of dispersant and nanotube type. In our study, three different dispersants, chlorosulfonic acid (CSA), N-Methyl-2-pyrrolidone (NMP), and sodium dodecyl benzene sulfonate (SDBS) were used to de-bundle carbon

* Reprinted with permission from "Dramatic electrical conductivity improvement of carbon nanotube networks by simultaneous de-bundling and hole-doping with chlorosulfonic acid" by Yeontack Ryu, Liang Yin, Choongho Yu, 2011. *Journal of Materials Chemistry*, 22, 6959-6964, Copyright [2012] by Royal Society of Chemistry.

nanotubes. SDBS is also known to be a good dispersant because the molecule has an aromatic ring that forms π-π bonding on nanotube surfaces. This improves the binding ability and surface coverage of SDBS,[79,80] separating nanotube bundles and keeping nanotubes de-bundled. NMP is another solvent that has been widely used,[81,82] and CSA has been recently studied for dispersing carbon nanotubes.[76,83,84]

5.2. Experimental procedure

5.2.1. Specifications of carbon nanotubes

The characteristics of carbon nanotubes may significantly vary, depending on nanotube synthesis methods (e.g., chemical vapor deposition (CVD), arc-discharge, and high pressure carbon monoxide (HiPco) methods). The synthesis method and condition determine the number of walls (e.g., single-/double-/multi-wall nanotubes), purity (e.g., amorphous carbon and metal impurity contents), the diameter of individual nanotubes, and defect density. Here, we tested carbon nanotubes of four different types: double-wall carbon nanotubes (DWNTs) and three different single-wall carbon nanotubes (SWNTs). They were synthesized by using CVD methods from Continental Carbon Nanotechnology (DWNT) and CheapTubes (CSWNT); an arc discharge method from Carbon solution (ASWNT); and the HiPco method from Unidym (HSWNT). According to the product information, DWNT (a purified grade called XBC grade) contains two concentric tubes with inner-tube diameters of 0.9-2.4 nm and outer-tube diameters of 1.5-3.0 nm with some single- and triple-wall tubes as impurities. ASWNT (a purified grade called P2) has metal contents (Ni and Y) ranging from 4 to 7 wt% and the

carbonaceous purity greater than 90 wt%. The average diameters of the individual and bundled tubes are 1.5 and 4-5 nm, respectively. The length of the bundles ranges from 500 nm to 1.5 μm. HSWNT has purity higher than 85 wt%. The mean diameter and length of individual tubes are 1 nm and 0.1-1 μm, respectively. CSWNT has purity higher than 90 wt% with ashes (<1.5 wt%), multi-wall nanotubes (>5 wt%), and amorphous carbon (<3 wt%) as impurities. The diameter and length of the tubes are respectively 0.8-2 nm and 5-30 μm.

5.2.2. Methods

The nanotubes were dispersed in CSA, NMP, or a SDBS-dissolved water solution, and then vacuum-filtrated to fabricate nanotube films. Electrical transport properties were measured for the films of twelve different kinds (i.e. 4 different nanotubes and 3 different dispersants). The electrical properties were strongly affected by sample preparation methods because the size of nanotube bundles and the degree of aggregation considerably varied. Scanning/transmission electron microscopy were used along with the Raman spectra to investigate the correlation of tube morphology (de-bundling), doping, impurity density, and defects with the electrical properties.

The nanotubes (10 mg) were dispersed in CSA (10 mL), NMP (20 mL), or deionized (DI) water (20 mL) with SDBS (20 or 50 mg). The CSA-nanotube solution was stirred for 24 hours in a closed vessel to minimize exposure to moisture in air. The NMP-nanotube and SDBS-nanotube solutions were ultrasonically dispersed with a pen-type sonic dismembrator (Fisher Scientific, FB 120) for 30 min. The amount of SDBS

with respect to the nanotubes was varied to identify the best ratios for high electrical conductivity. The optimum weight ratios of nanotube to SDBS were respectively found to be 1:2 for ASWNT and 1:5 for the rest (DWNT, HSWNT, and CSWNT). The as-prepared solutions were vacuum-filtrated by using hydrophilic polytetrafluoroethylene (PTFE) membranes with pores of 0.45 μm in diameter. The filtered CSA- and SDBS-dispersed nanotubes were washed with DI water, and the filtered NMP-dispersed nanotubes were washed with heptane and subsequently DI water by filtration. With these procedures, twelve different nanotube films made of CSA-, NMP-, or SDBS-dispersed DWNT, ASWNT, HSWNT, and CSWNT (i.e., CSA-/NMP-/SDBS-DWNT, CSA-/NMP-/SDBS-ASWNT, CSA-/NMP-/SDBS-HSWNT, CSA-/NMP-/SDBS-CSWNT) were fabricated.

The samples were made into strips with ~5 mm by ~12 mm, and mounted on a setup equipped with two T-type thermocouples and two copper wires for four-probe electrical and thermopower measurements at room temperature. Two line-shape silver electrodes were painted on both ends of the strips. In order to obtain film conductance, current (I) and voltage (V) were plotted by using an I-V sweeping method along the long edge of the samples. Voltages between two electrodes were measured at six different temperature differences between 0 and ±10 ℃, and then thermopower was extracted from the slope of the measured voltages with respect to the temperature differences. The coefficient of determination (R2) is higher than 0.99, and the temperature at 0 ℃ difference was ~23 ℃. The surface morphology of the carbon nanotube films was inspected by using a field-emission scanning electron microscope (SEM; FEI Quanta

600) and transmission electron microscope (TEM; JEOL JEM-2010). Raman spectroscopy (Horiba Jobin-Yvon Lab Ram IR) apparatus was also used with a laser of 633-nm wavelength to analyze the influence of the surfactant on the electrical properties of the nanotube films.

5.3. Results and discussion

Figure 5-1(a) shows the electrical conductivity of nanotube films made of the CSA-, NMP-, or SDBS-nanotube solutions. The highest electrical conductivity was measured to be ~1.7×10^6 S/m from CSA-DWNT. This electrical conductivity is orders of magnitude higher than those of typical carbon nanotube films[21,74,85,86] and composites,[1,3,9,87-90] and is the highest among those of previously reported carbon nanotube films, to our best knowledge. It was found that, regardless of nanotube types, CSA is superior to other dispersants for high electrical conductivity.

According to the morphology of the samples shown in Figure 5-2, the carbon nanotubes dispersed with CSA (a0~a4) have smaller diameter bundles with less impurities than those dispersed with NMP (b0~b4) and SDBS (c0~c4). The bundle diameter of CSA-DWNT was found to be ~20 nm and relatively uniform, as shown in the TEM image (a0), while the diameters of NMP-DWNT (b0) and SDBS-DWNT (c0) were ranged 50~100 nm and 20~100 nm, respectively.

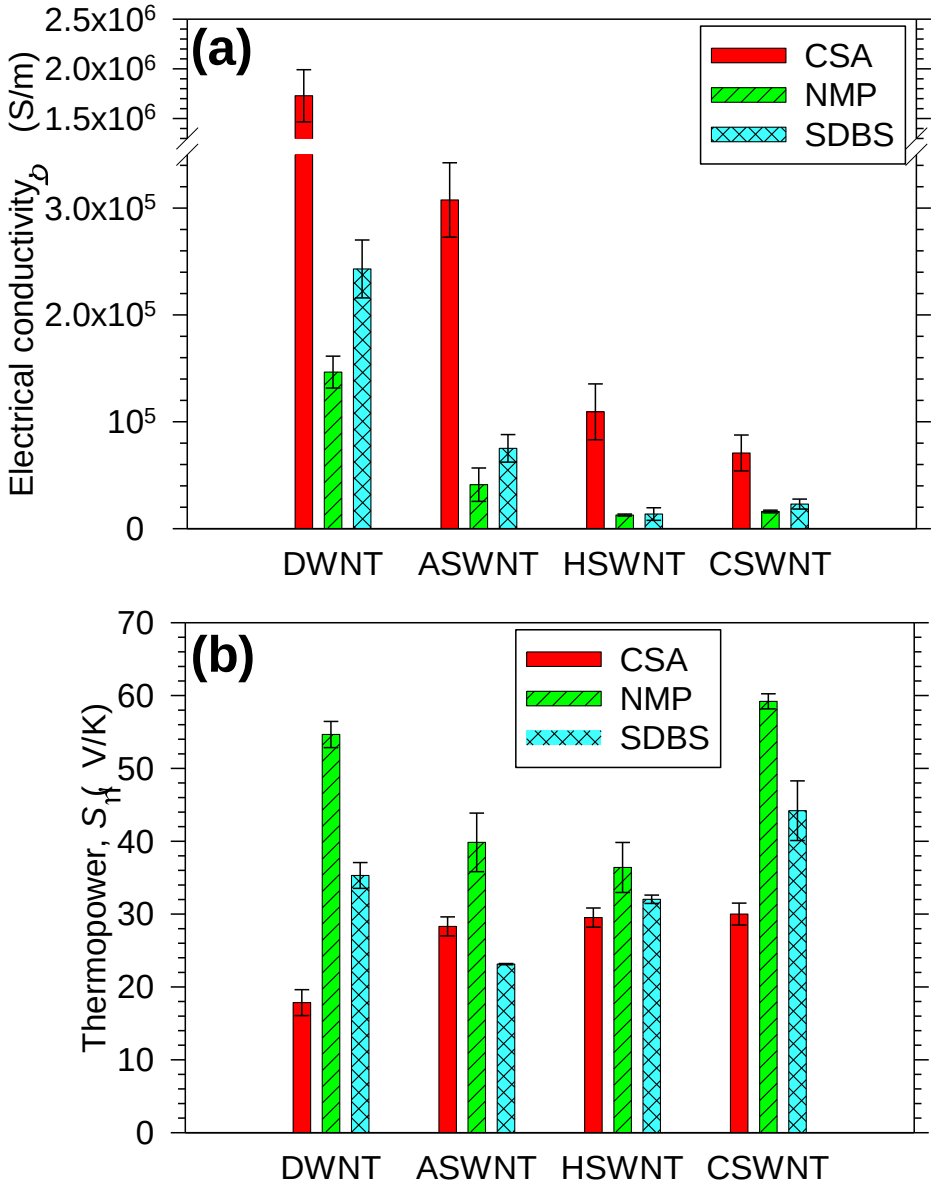

Figure 5-1 The electrical conductivity (a) and thermopower (b) of DWNT, ASWNT, HSWNT, and CSWNT films. The nanotubes were de-bundled with CSA (red bar), NMP (yellow single-hatched bar), or SDBS (cyan cross-hatched bar) solutions.

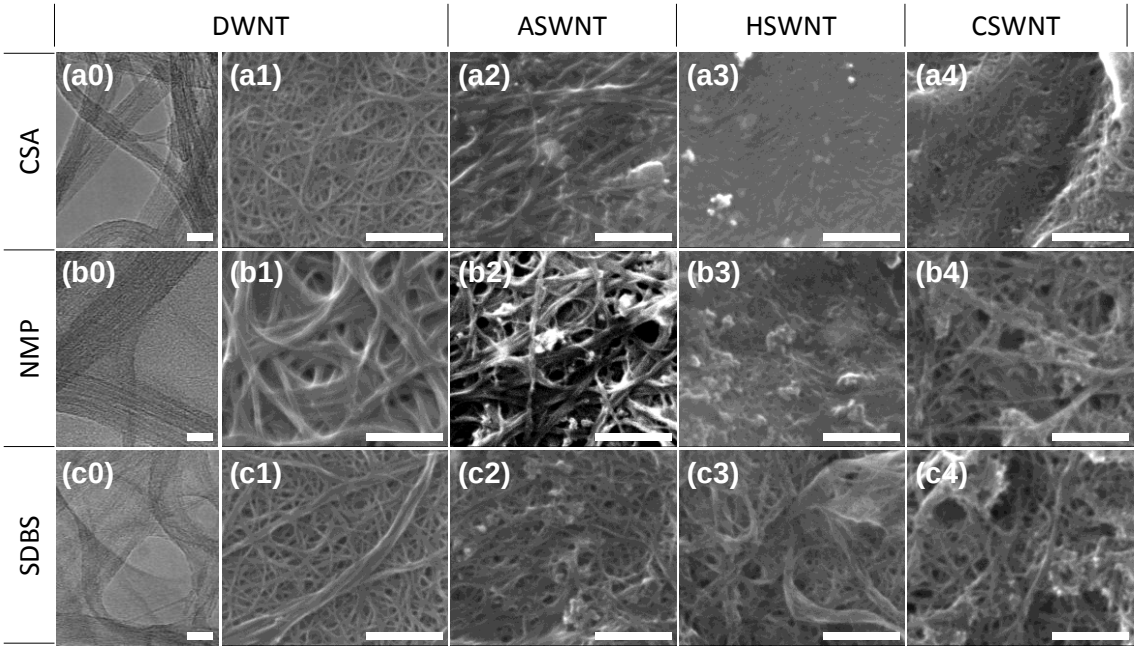

Figure 5-2 TEM images for CSA-DWNT (a0), NMP-DWNT (b0), and SDBS-DWNT (c0). SEM images for CSA-DWNT (a1), CSA-ASWNT (a2), CSA-HSWNT (a3), CSA-CSWNT (a4); NMP-DWNT (b1), NMP-ASWNT (b2), NMP-HSWNT (b3), NMP-CSWNT (b4); SDBS-DWNT (c1), SDBS-ASWNT (c2), SDBS-HSWNT (c3), SDBS-CSWNT (c4). The scale bars for the TEM and SEM images respectively represent 20 nm and 500 nm.

The samples made of ASWNT, HSWNT, and CSWNT also showed that CSA also removed impurities better than NMP and SDBS. When nanotubes are spearated into smaller diameter bundles, the resulting samples have more tube-tube junctions and higher packing density than those made of larger diameter bundles. In carbon nanotube filled composites, the junction resistance is one of the most crucial factors that suppress the electrical conductivity.[1,3,9,91] Smaller bundles create a large number of junctions between the bundled tubes, as evident by comparing (a1) and (b1), making less electrically resistive paths across the film. When the bundles are crossed each other, the actual contact area between them is very small. The contact may limit electron transport

significantly. When the bundle diameter is large, more electrons need to pass through the small constricted junctions. The total contact resistance is inversely proportional to the number of the junctions but is proportional to the contact resistance from the individual junction. The contact resistance for the individual junction is likely to be dependent on the dispersant. This implies that the electrical properties are a strong function of the actual carrier density that participates in the electrical conduction rather than the intrinsic carrier density of individual nanotubes. Less porosity (i.e., a high packing density) may also increase electrical conductivity due to the geometrical factor, and less impurities reduces electron scattering events that are responsible for suppressing electron transport. Furthermore, intercalation of hydrogen ions between the nanotubes or oxidation of carbon nanotubes by CSA cause hole-doping into nanotubes, raising the electrical conductivity.[83]

NMP is widely used to disperse carbon nanotubes, but NMP was particularly not very effective in separating DWNT bundles (Figure 5-2(b1)) compared to CSA and SDBS. When the bundle diameter is larger, electrical conductivity was measured to be lower, as shown in Figure 5-1(a) (NMP-DWNT). NMP-ASWNT (Figure 5-2(b2)) also shows worse dispersion than SDBS-ASWNT, resulting in lower electrical conductivity. On the other hand, NMP and SDBS have similar influence on the dispersion of HSWNT and CSWNT, resulting in similar conductivities. Slightly higher electrical conductivities from SDBS samples compared to NMP samples may be due to hole-doping effects (attracting electrons to the surface) from sodium ion in SDBS.[79]

Thermopower (Figure 5-1(b)) was measured together with the electrical conductivity, showing a typical trend that is inversely proportional to electrical conductivity, except ASWNT. The values are within typical ranges, 10~60 μV/K for carbon nanotube based films[11,15,92] and composites[1,3,10,69] whose thermopower values are strongly dependent on sample preparation methods (e.g., nanotube type, surfactant, and composite matrix). In general, when the carrier concentration is raised, thermopower diminishes and electrical conductivity increases. For the samples made of the same tubes, the total number of carriers should be identical but the carriers that actually participate in the electrical transport would vary depending on the total contact resistance at the tube-tube junctions as well as doping. While CSA makes the bundle diameters smaller, NMP and SDBS did not make noticeable differences in ASWNT, HSWNT, and CSWNT. Nevertheless, thermopower with NMP shows higher values than others. It is likely that NMP intervene at the junctions and strongly interfere with electron transport, increasing thermopower due to filtering low energy electrons.[9-11] Among the four different tubes, CSWNT shows higher thermopower than others. This may be due to the catalyst impurities, which may scatter low energy electrons.[11,66] SEM images of CSWNT in Figure 5-2 depict small particle impurities of relatively high concentrations. The small diameters from CVD processes[93] (i.e., containing more semiconducting tubes) may be another reason.

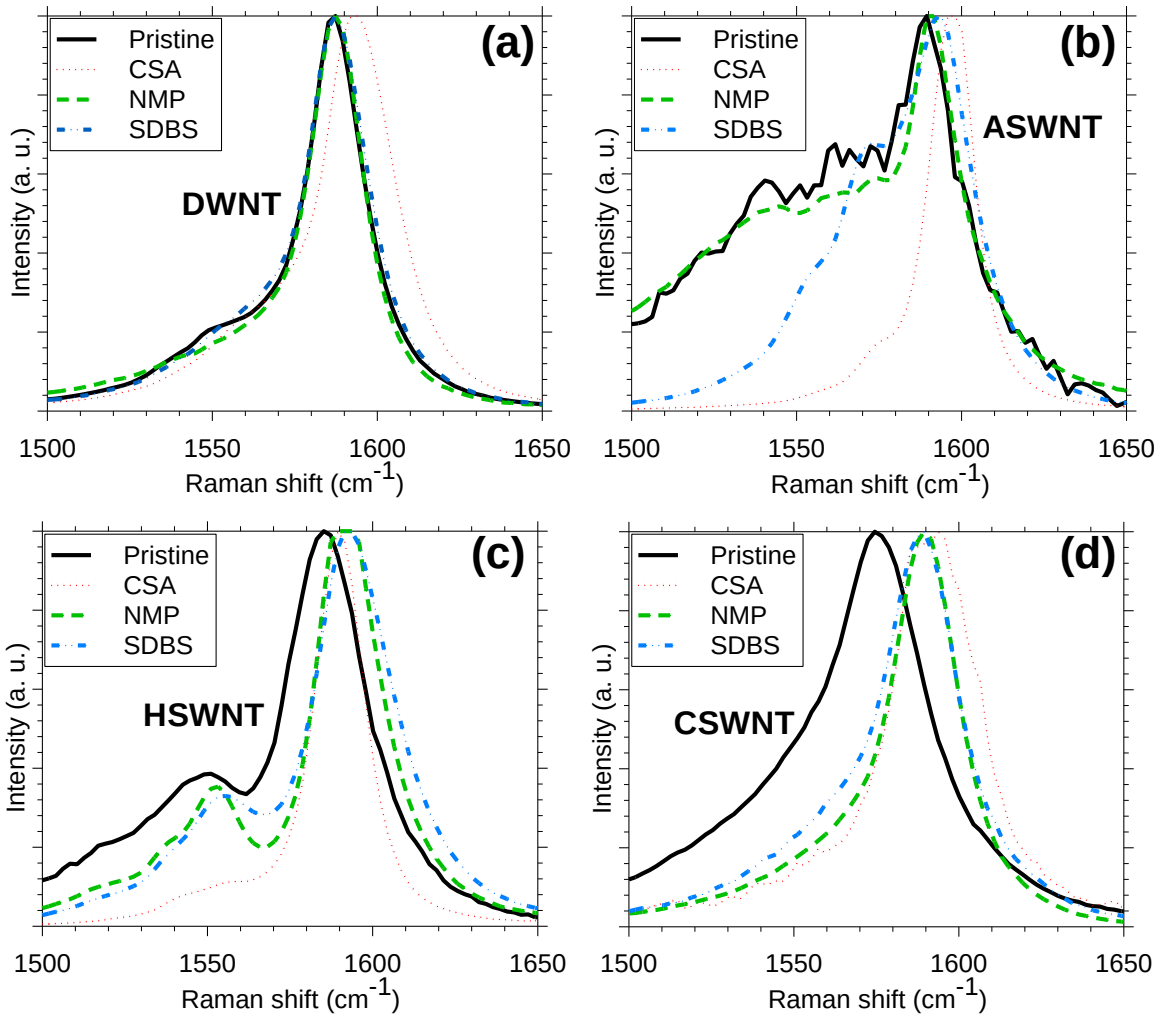

Figure 5-3 G-band Raman spectra with 633-nm laser excitation for DWNT (a), ASWNT (b), HSWNT (c), CSWNT (d) films when the nanotubes were de-bundled with CSA (red dotted line), NMP (green dashed line), or SDBS (blue dash-dotted line) compared to those of prinstine nanotubes (black solid line).

CSA, NMP and SDBS did not only vary the electrical conductivity of the nanotube samples, but also altered the Raman spectra, as shown in Figure 5-3. SWNTs and DWNTs have G^+ mode, which is related to carbon atom vibrations along nanotube axis, near 1590 cm^{-1}.[94] G^- mode of SWNTs occurs near 1550~1570 cm^{-1}, which is related to carbon atom vibrations along circumferential direction of nanotubes. SWNTs

show two specific line-shapes, called the Breit-Wigner-Fano (BWF) line-shape for metallic nanotubes and the Lorentzian line-shape for semiconducting nanotubes, respectively.[94] While the Lorentzian line-shape indicates symmetric G^- and G^+ modes, the BWF line-shape is asymmetric with a higher intensity for the G^+ mode. While pristine ASWNT and HSWNT show distinct G^- modes, only G^+ mode was observed from CSWNT. The suppressed G^- mode from CSWNT may be due to a large percentage of semiconducting tubes, resulting in relatively high thermopower with low electrical conductivity, as shown in Figure 5-1.

When nanotubes were dispersed with CSA, up-shifted G^+ modes compared to those of pristine DWNTs and SWNTs were observed. This change in the G^+ mode generally occurs with hole-doped or de-bundled nanotubes,[95,96] which concide with higher electrical conductivity in Figure 5-1 and smaller bundle diameters in the SEM images (Figure 5-2). For both ASWNT and HSWNT, the G^- mode in the BWF line-shape after the CSA treatment was suppressed, indicating typical signatures for hole-doping or de-bundling nanotubes.[24,94,97] On the other hand, NMP and SDBS induced relatively small changes in the G^- mode (see the relatively low electrical conductivity in Figure 5-1).

In Figure 5-3(b), the G^+ and G^- modes of SDBS-ASWNT is respectively slightly more up-shifted and suppressed compared to those of NMP-ASWNT. Thses features would be related to the smaller bundle diameters and higher electrical conductivity from SDBS-ASWNT. Meanwhile, NMP and SDBS did not make a significant difference in the G^+ modes for HSWNT and CSWNT, which explains similar electrical conductivity

and bundle diameters. For DWNT, the two spectra with NMP and SDBS were barely changed, presumably due to the interactions between the inner and outer walls.

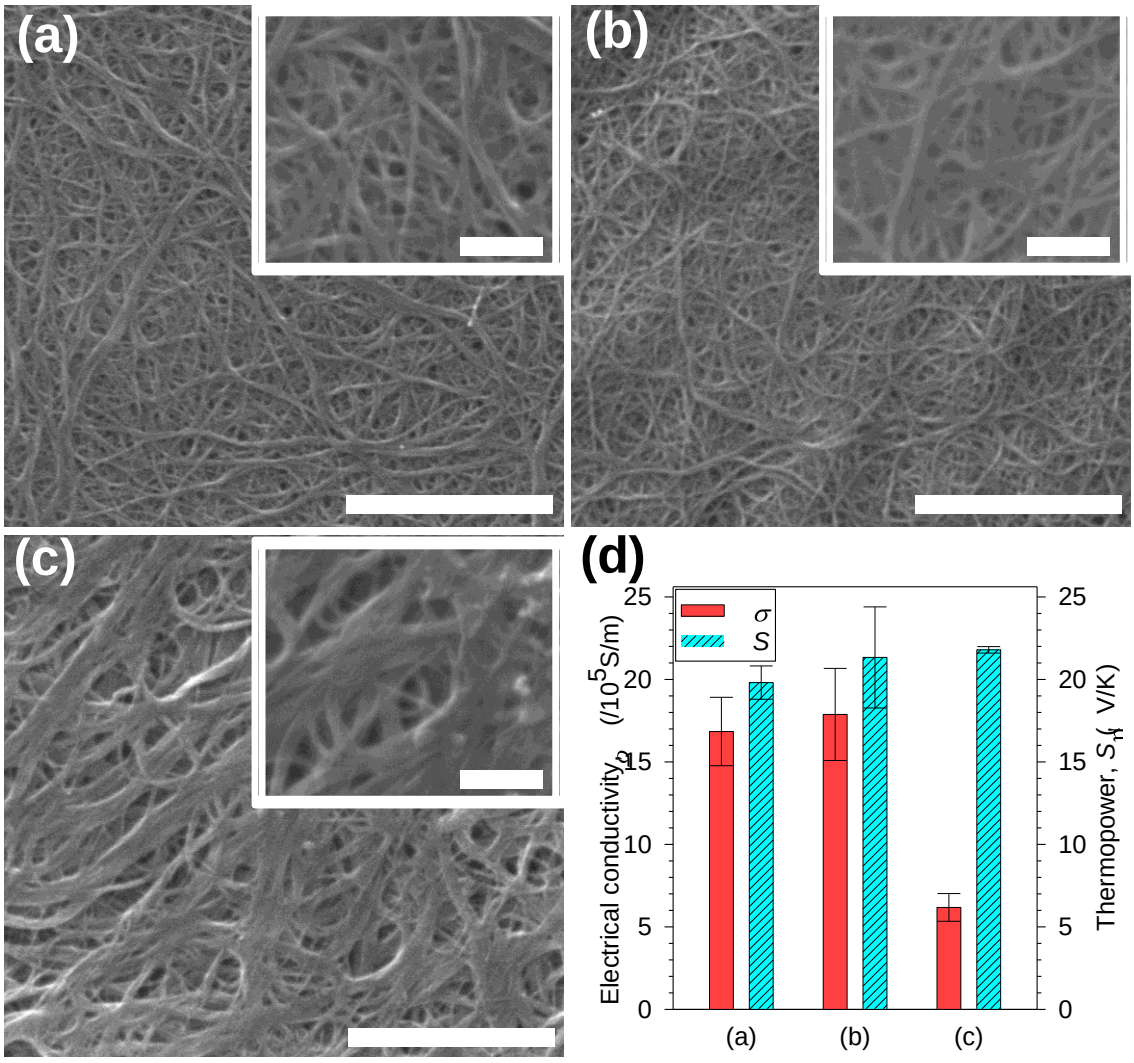

Figure 5-4 SEM images of the films made of DWNTs dispersed by CSA. DWNTs were stirred with CSA for 3 hours in a closed vessel (a), 24 hours in a closed vessel and then expose the CSA-DWNT solution to room air (moisture) for ~1.5 hours during the filtration process (b), and CSA-DWNT were stirred for ~96 hours and filtrated for ~20 hours with a vessel open to room air (moisture) (c). All scale bars except for the insets represent 1 µm. The insets represent 200 nm. (d) The electrical conductivity (σ) and thermopower (S) of the CSA-DWNT films shown in (a), (b), and (c).

The CSA-DWNT synthesis condition, which resulted in the highest electrical conductivity, was further investigated so as to study the influence of the sample preparation conditions on dispersion and electrical properties. The stirring/sonication time, CSA volume, filtration time, and exposure to moisture were tested. First, the stirring time was reduced from 24 hours (the sample in Figure 5-2(a1)) to 3 hours. The 3-hour stirring sample (Figure 5-4(a)) contains nanotube bundles of slightly bigger diameters than the sample with 24 hour stirring (Figure 5-2(a1)), but most of them have similar diameters (10~20 nm). The electrical conductivity and thermopower were also measured to be high, ~1.7×10^6 S/m (Sample (a) in Figure 5-4(d)), which is very close to those of the 24-hour stirring sample (CSA-DWNT in Figure 5-1(a)). Note that the exposure of CSA to moisture (room air) was minimized by performing the experiments with closed containers.

On the contrary, CSA was intentionally exposed to air during the filtration process as well as both stirring and filtration processes since CSA is very reactive to moisture, resulting in HCl and H_2SO_4. When the CSA-nanotube solution was stirred for 24 hours in a closed vessel and then filtrated for ~1.5 hours with air exposure, the dispersion was very similar to the sample without air exposure, as shown in Figure 5-4(b). In addition, the electrical conductivity and thermopower are also similar to those of 24- and 3-hour stirring samples (CSA-DWNT in Figure 5-1(a) and sample (a) in Figure 5-4(d)). We also used sonication instead of stirring, but we did not observe any improvement in de-bundling nanotubes. On the other hand, when the CSA-DWNT solution was stirred and filtrated in an open container for a longer time period, the

dispersion and the electrical properties were altered, as shown in Figure 5-4(c) and sample (c) in Figure 5-4(d). In this case, DWNT of 10-mg was dispersed in CSA of 100-mL to ensure the dispersion is not limited by the amount of CSA. Then, the solution was continuously stirred for ~96 hours and filtrated for ~20 hours. The large reduction in electrical conductivity (~6×10^5 S/m) is likely due to the large-diameter bundles (as big as a few 100 nm in diameter) that deter electron transport at the junctions. These results indicate that de-bundling of nanotubes is crucial in improving electrical conductivity.

Thermopower values, however, were more or less unchanged, indicating it is close to the intrinsic property of DWNT. This is because electrons travel along least resistive paths and thermopower does not depend on the geometrical parameters. In other words, thermopower is not considerably affected even though a portion of a material becomes electrically resistive as long as the material contains conductive paths. For example, thermopower of a composite that is made of two different materials can be described as[15,98]

$$S_{composite} = \frac{\left(S_1/R_1 + S_2/R_2\right)}{\left(1/R_1 + 1/R_2\right)} \tag{4}$$

where R_1 and R_2 as well as S_1 and S_2 respectively represent the electrical resistances and thermopowers of two different materials. Suppose that material 1 and 2 are respectively highly conductive and resistive portions in a composite. Then, $R_1 << R_2$, $S_{composite} \sim S1$, resulting in negligible influence from the resistive portion.

5.4. Conclusion

In summary, DWNTs and SWNTs grown by CVD, Arc, and HipCo methods were de-bundled by using three different dispersants, CSA, NMP, and SDBS to study the influence of de-bundling and doping on electrical transport properties of carbon nanotube films. SEM, TEM, and the Raman spectroscopy were utilized to investigate the correlation between the electrical properties (electrical conductivity and thermopower) and morphology/doping of the films. When DWNT films were made with CSA, electrical conductivity and thermopower were measured to be ~1.7×10^6 S/m and ~18 μV/K, respectively. The electrical conductivity is the highest among those of carbon nanotube films and composites, to our best knowledge. We believe that the dramatic improvement in electrical conductivity is attributed to effective de-bundling and doping by the strong acid molecules intercalated between nanotubes, as confirmed by both SEM/TEM images and Raman spectra. Regardless of nanotube types, nanotube films made with CSA showed higher conductivities than those from NMP- and SDBS-solutions. On the other hand, the films made of the nanotubes dispersed by NMP have higher thermopower values (up to ~60 μV/K) than those of the samples made with CSA and SDBS. This is likely to be due to the inferior dispersion without doping effects. CSA-treated samples contain fewer impurities, yielding relatively low thermopower. It was found that the de-bundling significantly affects electrical conductivity, but thermopower is weakly correlated with the dispersion.

6. STUDY 5: THERMAL CONDUCTANCE MEASUREMENT IN GOLD NANOPARTICLE DECORATED CARBON NANOTUBE BUNDLES

6.1. Objective

Study of electron transport properties in surface-modified carbon nanotubes has been performed only in nanotube films forming network with multi-direction. It verifies how the transport properties are changed when nanotube surface were modified especially decorated by nanoparticles. But the results do not reflect on characteristics of individual carbon nanotubes directly because the films have too many junctions as well as all nanotubes can't be separately characterized before and after a surface modification. In addition to this, thermal properties were not measured from the films yet because it is not easy to measure them from thin films. They are also required to estimate ZT value for thermoelectric. Therefore, it is necessary to investigate the change of thermal conductance before and after surface modification.

6.2. Carbon nanotube synthesis

Carbon nanotubes were synthesized by wet-assisted chemical vapor deposition (CVD) method. First, Fe of 5nm and Al of 10 nm respectively in thickness were deposited on silicon wafer by a thermal evaporator. In order to grow nanotubes, a 1 inch tube furnace was prepared with proper gas connection lines as shown in Figure 6-1.

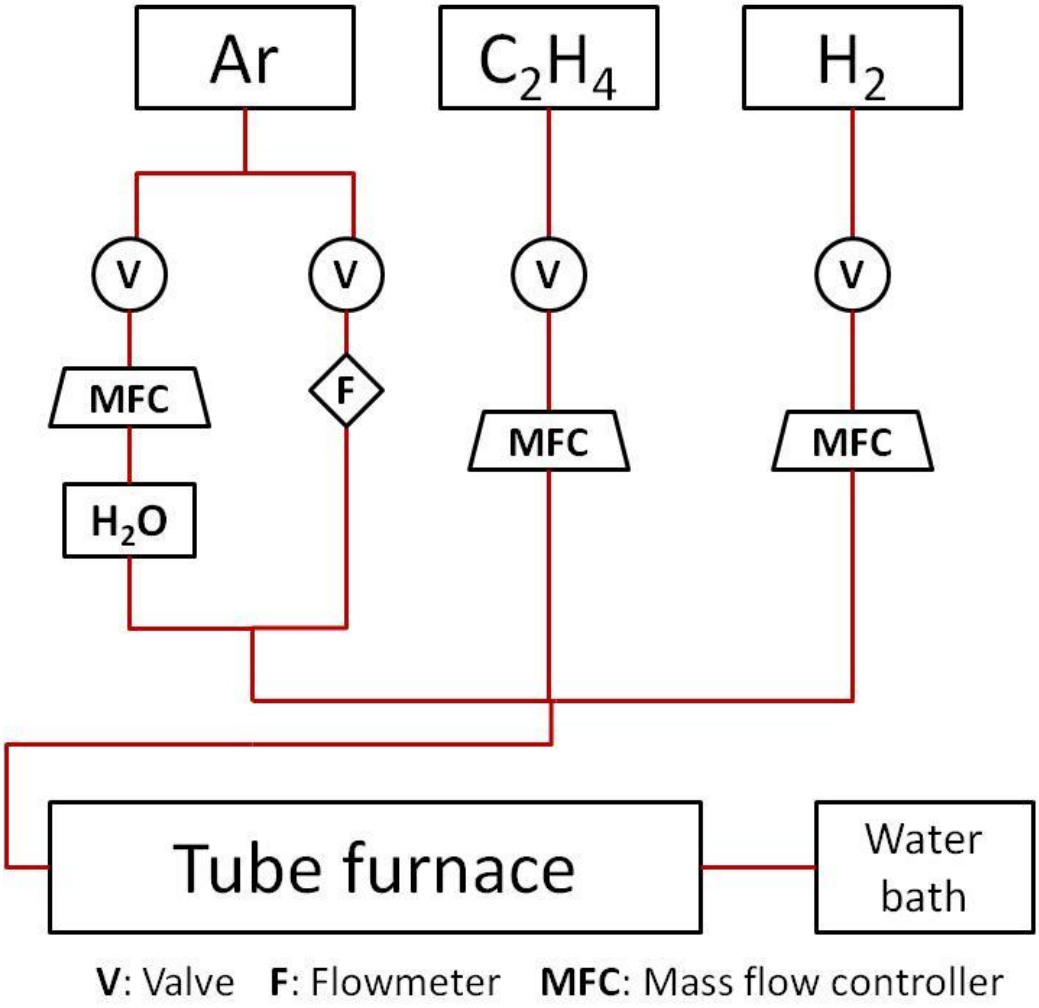

Figure 6-1 A schematic diagram of carbon nanotube synthesis.

The substrated was placed on the center of the tube and then moisture level inside was reduced to ~300 ppm by flowing Ar. Ar of 80 sccm and H_2 of 30 sccm were delivered during ramping from a room temperature to 750 C for 10 min. When a temperature reaches to 750 ℃, C_2H_4 of 100 sccm was purged out together with wet Ar of 5 sccm. The reaction was maintained for 20 min and subsequently all gases were turned off except Ar while the sample was cooled down naturally. 400 um carbon nanotube forest

in length were obtained from the synthesis as shown in Figure 6-2. This may have more opportunity to bridge nanotubes properly on the microdevice even if they are broken by some sonication.

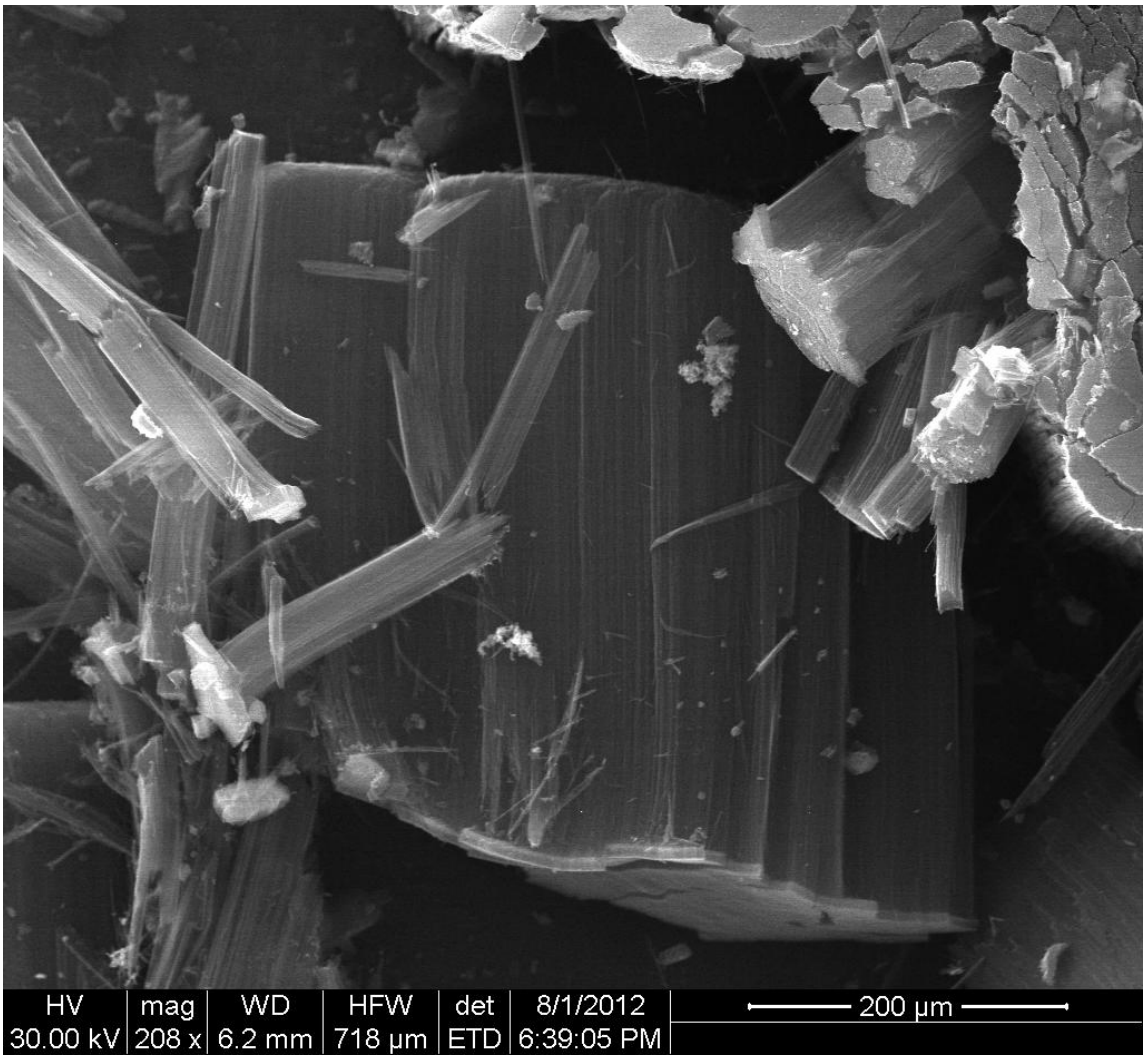

Figure 6-2 Carbon nanotube forest grown by a wet-assisted CVD technique.

6.3. Thermal and electrical measurement

In this study, CVD grown multiwalled nanotube bundle was assembled on microdevice to measure the properties. As-prepared microdevice was installed to a cryostat with a vacuum level better than 1×10^{-3} Torr and was connected to two SR830 lock-in amplifiers and a data acquisition (DAQ) board. The temperature of the microdevice was maintained at room temperature during measurement by a temperature controller connected to the cryostat.

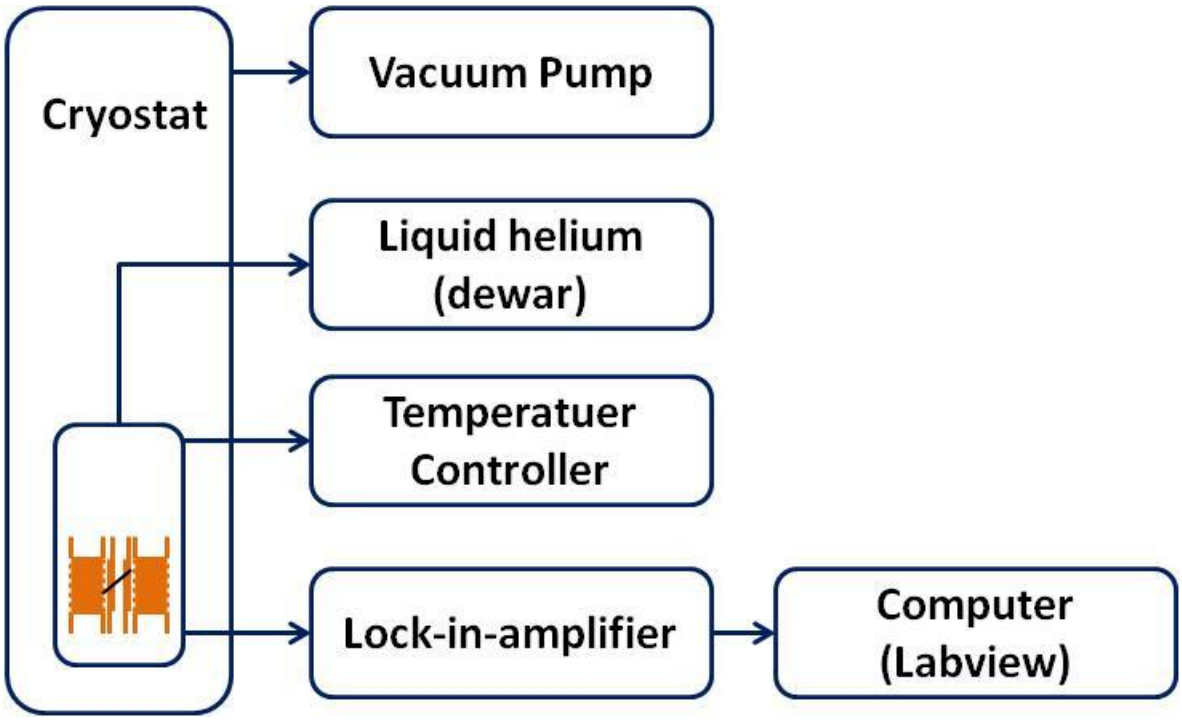

Figure 6-3 A schematic diagram of the experimental setup for measuring the thermal and thermoelectric properties of carbon nanotubes.

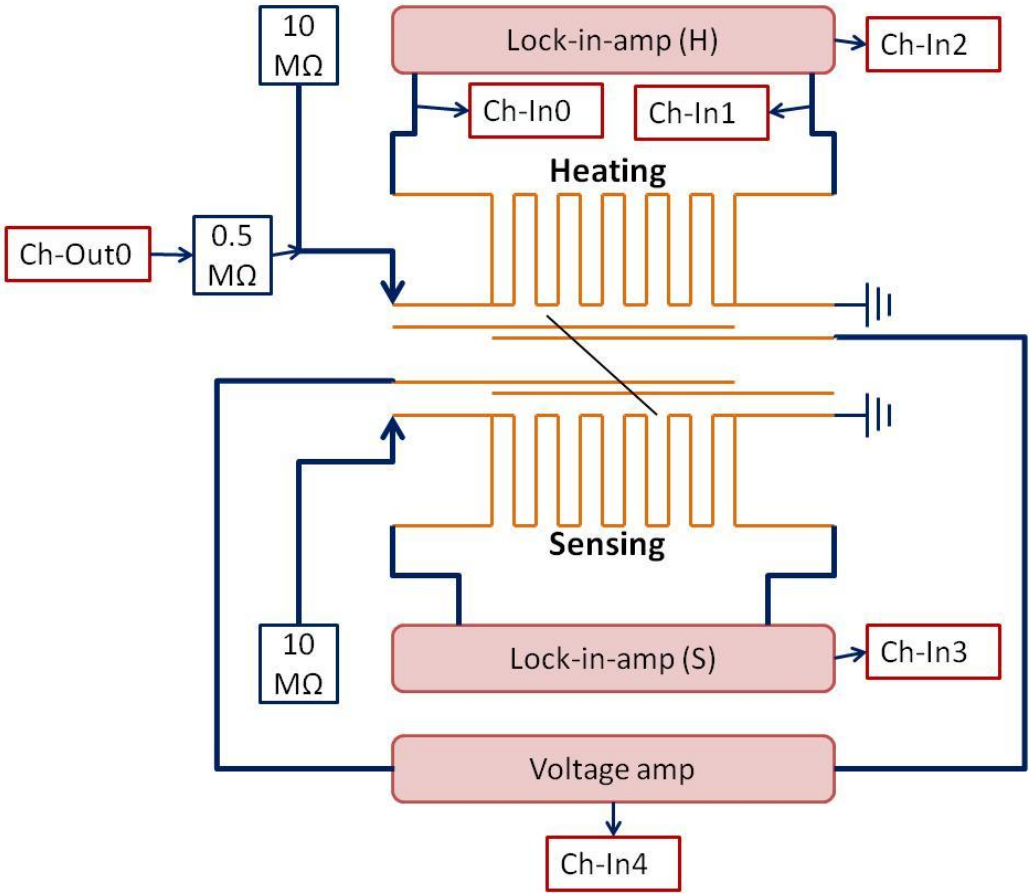

Figure 6-4 A schematic diagram of the connection of the measurement equipment to the microdevice.

Figure 6-3 describes the connection of the measurement equipment to the microdevice. For thermal conductance measurements of nanostructures, one of the heater lines was coupled to DC current (Vout: Ch0) using a DAQ board to raise the temperature of the lower membrane (from D to A). Meanwhile, to measure temperature rises in the membranes, AC current was passed through the heater lines (from D to A and from G to K) and voltage drops across the lines were measured between B and C, and H and J. To measure the Seebeck coefficient of nanostructures, a voltage difference across the nanostructure (E and F) was measured by using a voltage amplifier. In

addition, the electrical conductance of the nanostructure was measured using a DC current supplied (from E to F) using a DAQ output port (Vout: Ch1) with a current amplifier. All data were recorded to Ch0~5.

6.4. Experimental procedure

Carbon nanotubes grown by CVD were mixed with ethanol and sonicated for 5 min to avoid broken nanotubes. Several drops of the nanotube solutions were dried on a glass slide. Probe station with an optical microscope and 4 micromanipulators was assembled. Carbon nanotube bundle was delivered by a micromanipulator probe and placed along the microdevice membrane, and subsequently the device was annealed at 650 ℃ under of vacuum level of 0.01 torr for 1 hour to reduce contact resistance between electrodes and nanotubes. After measuring the properties of the samples, they were immersed into 10 mM $HAuCl_4$ of ethanol solution for 5 min and subsequently transferred to ethanol and hexamethyldisilazane (HMDS) in order carefully. Au ions were expected to be reduced and attached to carbon nanotube surface spontaneously due to difference of reduction npotentials between Au and nanotubes. The purpose of this process is to avoid detachment of nantoubes due to moving of the membrane which may be attributed to surface tension occurred when solution is dried. Thermal conductance measurement was performed again for the Au nanoparticle decorated sample with the same method described above.

6.5. Results and discussion

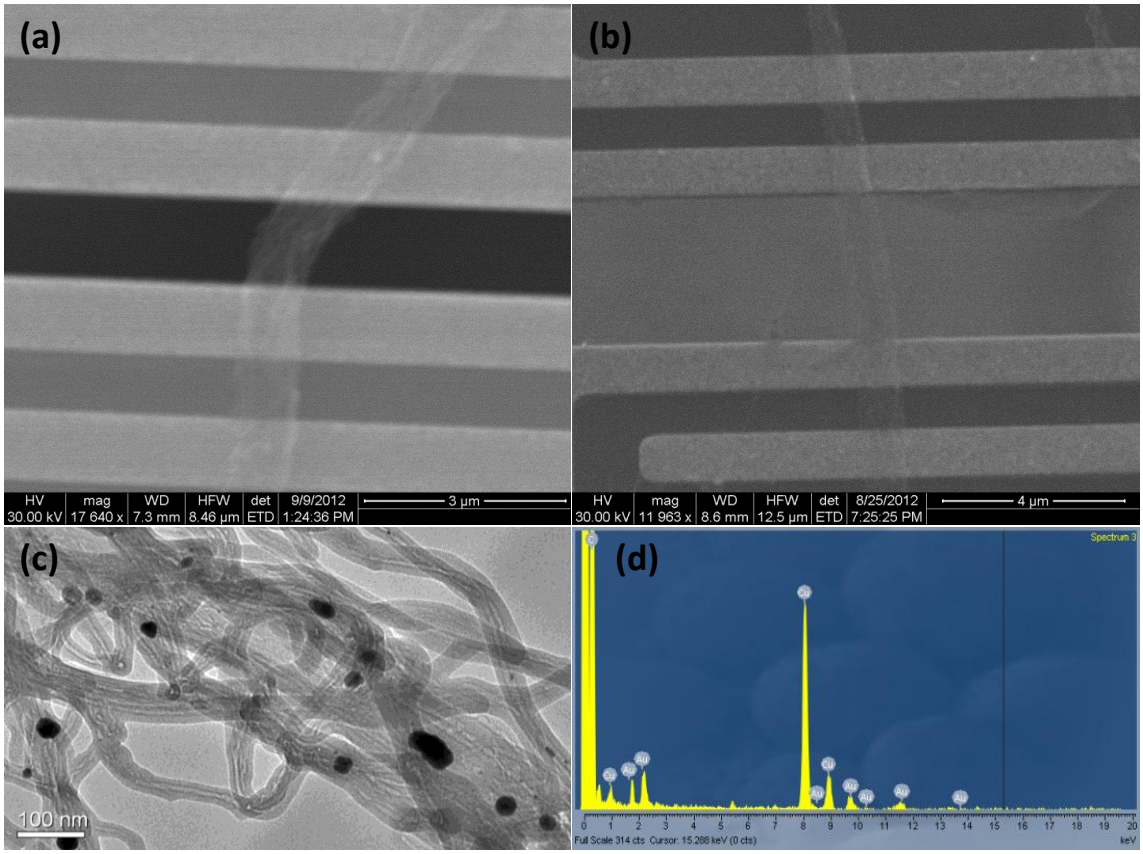

Figure 6-5 SEM images of (a) pristine carbon nanotube bundle and (b) Au-carbon nanotube bundle bridged on microdevice. (c) TEM image and (d) energy dispersive X-ray spectroscopy (EDS) analysis of Au-carbon nanotube bundle.

As shown in (a) and (b) of Figure 6-5, pristine and Au-decorated nanotube bundles were bridged along the four platinum electrodes. In order to separate nanotube from heater lines, a ~3V was supplied from a KEITHLEY 2400 sourcemeter between heater line and electrodes until a current dropped to zero. Or Focused-ion beam (FIB) was also utilized for the same purpose. Figure 6-5(c) is TEM image of Au-carbon nanotube bundles where several Au particles with 5~20 nm in diameter were decorated along the nanotube surface. The nanotube looks like multi-walled carbon nanotube

(MWNT) and Au on carbon nanotube is confirmed by energy dispersive X-ray spectroscopy (EDS) in Figure 6-5(d).

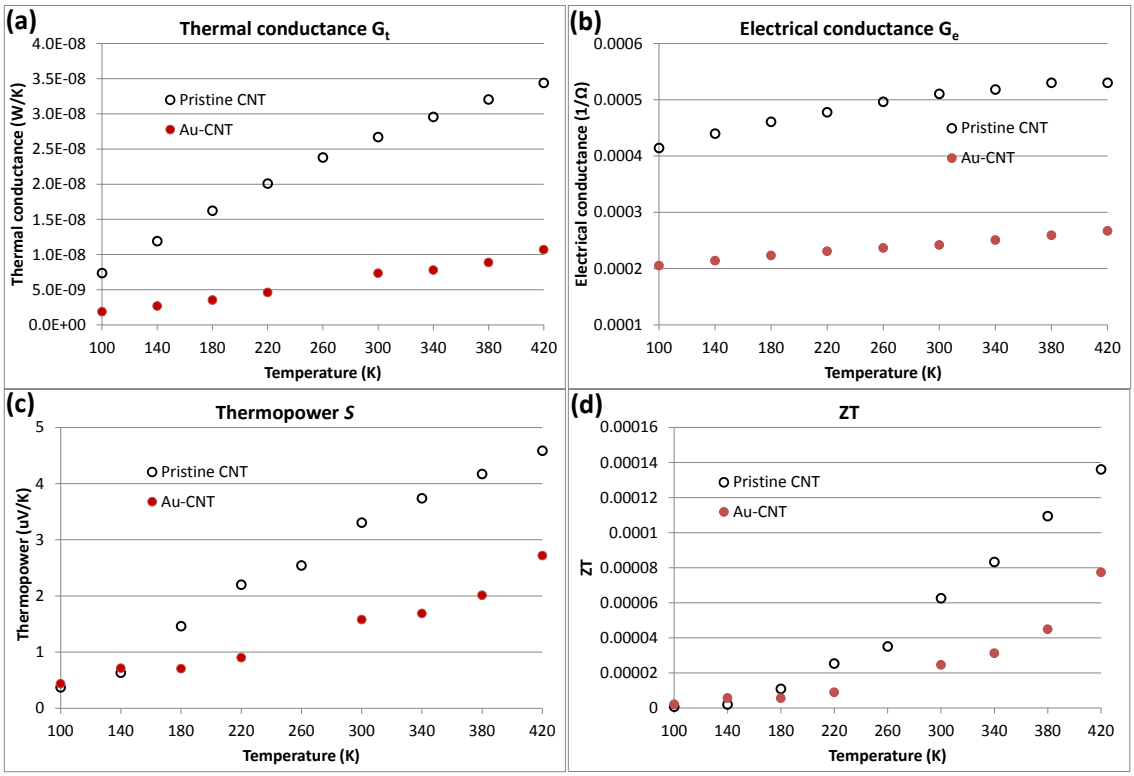

Figure 6-6 (a) Electrical conductance G_e, (b) Thermal conductance G_t, (c) Thermopower *S*, and (d) *ZT* for pristine CNT and Au-CNT bundles.

As characterized in SEM of Figure 6-5, it doesn't seem to be easy to have accurate analysis in nanotube dimension because nanotube number, density, length of single nanotube, or bundle shape are all the things to be considered for electrical and thermal conductivities. Thus, herein, electrical or thermal conductance not conductivity was calculated from the measurement. Because thermopower *S* is not limited by nanotube dimension, a thermoelectric figure of merit *ZT* can be easily estimated as the following.

$$ZT = \frac{\sigma}{\kappa} S^2 T = \frac{l}{RA} \frac{\Delta T A}{Q l} S^2 T = \frac{G_e}{G_t} S^2 T \quad (4)$$

Here, l, A, Q, G_e, and G_t are length, area, heat, electrical conductance, and thermal conductance, respectively. Figure 6-6 presents electrical and thermal conductance, thermopower, as well as ZT value with different temperature from 100K to 420K for both pristine CNT and Au-CNT bundles. First, note that electrical conductance G_e increases with temperature which is a typical behavior of nonmetallic materials. In multiwall nanotubes, electrons of outer shell are dominant in conductance and they can travel to another nanotube shell by hopping. Because there exists an energy barrier for the thermally activated conduction between the shells[99], electrical resistivity is reduced at higher temperature. Figure 6-6(a) shows increase of electrical conductance with temperature for both pristine CNT and Au-CNT. On the other hand, thermal conductance of Au-CNT is lower than in all temperature range than that of pristine CNT from Figure 6-6(b). When we assume the nanotube bundles as a single cylindrical shape of nanowire, calculated thermal conductivities had the same trend with the conductance result. This is likely to a reduction of thermal conductivity by a phonon scattering due to mass difference between Au and Carbon. Thermal conductance typically increases with temperature for metallic materials because free electrons, major carriers, are thermally activated and their mobility is enhanced. In addition, the increasing rate of thermal conductance with temperature is smaller in Au-CNT. This is attributed that a scattering generated by Au decoration reduces electron mobility. Thermopower was also measured and shown in Figure 6-6(c), indicating a typical metallic behavior of MWNT with

increasing property as increase of temperature. Finally, *ZT* value was estimated in Figure 6-6(d) by combining all thermoelectric parameters measured and calculated. For both pristine CNT and Au-CNT, *ZT* seems to increase with temperature exponentially. The plot shows ZT is similar in lower temperature range for both and is higher in higher temperature range for pristine CNT. This indicates that Au-CNT may be worse in thermoelectric application at least within high temperature range. This is consistent with reduction of power factor in Au-CNT film as seen in study 1 of this dissertation. However, it is also worth to try smaller and more Au particle decoration on carbon nanotube for *ZT* enhancement because a current sample used in this study shows somewhat large and rare Au nanoparticles on nanotube surface as shown in Figure 6-5(c). Another candidate should be Cu decoration which already showed enhancement of power factor in study 1.

6.6. Conclusion

Carbon nanotubes were synthesized by wet-assisted CVD method and long nanotube forest with ~400 μm in length was obtained. The nanotube bundles was extracted and delivered on a microdevice by an aid of a micromanipulator probe for measurement of thermophysical properties. Electrical and thermal conductances, and thermopower were automatically measured in cryostat connected with temperature controller, vacuum pump, lock-in-amplifier, voltage amplifier, and labview operating system. BeDue to a phonon scattering in Au-CNT, it has a tendency of lower thermal conductance and it slower increase with a temperature compared to pristine CNT.

Overall *ZT* shows exponential increase with a temperature for both pristine CNT and Au-CNT, and it becomes larger as increase of temperature for pristine CNT.

7. CONCLUSION (FUTURE DIRECTION)

Nanoparticle decoration on carbon nanotubes was employed to modulate their electrical conductance and thermopower and thereby improved the thermoelectric power factor. A series of experiments at different Cu ion concentrations and reaction time periods were systematically performed in order to find optimum nanoparticle formation conditions and corresponding electronic transport changes for better thermoelectric power factor. Transport measurement results show that electronic properties can be considerably altered and modulated, resulting in 2-fold improvement in the thermoelectric power factor with 1 mM/30 min reaction. This transport behavior is believed to be from the changes in the Fermi level as a result of electron exchanges between reduced metals and nanotubes. Thermopower improvement after copper decoration can be attributed to the enlarged gap between the Fermi level and the mean of differential electrical conductivity. Such behaviors often appear when the Fermi level is shifted toward the spike-shape density of states in nanotubes due to anisotropic differential electrical conductivity. This study demonstrates that the thermoelectric power factor can be considerably increased by properly locating the Fermi level of carbon nanotubes with nanoparticles, providing promising opportunities of developing efficient organic thermoelectric materials as well as various electronic materials of desired properties.

Carbon nanotubes were largely decorated with organic or inorganic nanomaterials in order to obtain desired electrical transport properties such as a high

electrical conductivity or an n-type thermopower. The electrical conductivity of double-wall carbon nanotubes (DWCNTs) decorated with tetrafluoro-tetracyanoquinodimethane (F4TCNQ) was increased up to 5.9×10^5 S/m, and single-wall carbon nanotubes (SWCNTs) were converted from p-type to n-type with a large thermopower (−58 μV/K) by using polyethyleneimine without vacuum or controlled environment. We believe these transport property changes can be attributed to charge interactions resulted from the difference between the work functions/reduction potentials of nanotubes and nanomaterials. This study shows a first step toward the synthesis of both n-type and p-type conductors with carbon nanotubes, which are essential to thermoelectric energy conversion applications.

In addition, more nanomaterials were decorated on carbon nanotube thin films for the application of transparent and conductive electrode. When organic tetrafluoro-tetracyanoquinodimethane (F_4TCNQ) molecules were incorporated into the nanotube films, sheet resistance was reduced to ~50 % of those from the pristine SWNT and DWNT films. Larger improvements were observed with Au nanoparticle decoration or $HNO_3/SOCl_2$ dipping processes. The sheet resistances were measured to be 42 Ω/sq at 75 % of transmittance for $HNO_3/SOCl_2$-treated DWNT films and 64 Ω/sq at 77 % for Au-incorporated DWNT films, making their electrical conductivities 200~300 % better than those of the pristine DWNT films. The relative influence of various dopants, F_4TCNQ, Au, and $HNO_3/SOCl_2$ as well as microwave irradiation on the optical and electrical properties was identified by using Raman and UV-Vis-NIR spectra.

Electron/phonon transport phenomena in bulk-scale carbon nanotubes are governed by the junction properties in such nanotube networks. For instance, the excellent electrical properties of an individual nanotube are dramatically deteriorated when they are bundled or made into bulk materials for practical applications. Our study employed several different dispersing agents including sodium benzenosulfonate (SDBS), chlorosulfonic acid (CSA), N-Methyl-2-pyrrolidone (NMP), and graphene oxide (GO) sheets for various nanotubes such as single-/double-/multi- walled carbon nanotubes. As-dispersed carbon nanotube solutions were vacuum-filtrated and then properly post-processed to minimize the effect of the agents. Electrical conductivity, thermopower, and thermal conductivity of the prepared films were measured. Raman spectroscopy and Fourier transform infrared spectroscopy (FTIR) were also carried out for characterizing the incorporated agents as well as analyzing the change in the junction properties of the nanotube networks. A very large enhancement of electrical conductivity was observed from CSA-treated samples regardless of nanotube types. The electrical conductivity is as high as $\sim 1.3\times 10^{6}$ S/m, which is orders of magnitude higher than other typical nanotube-based bulks, from double-walled carbon nanotube films. We also investigated interactions between the nanotubes and the dispersants in order to find their influence on the transport properties.

All studies described above are for carbon nanotube films or mats. Electron transport properties of carbon nanotubes were dramatically altered by decorating nanomaterials on the surface of nanotubes, changing the decoration process, and

debundling of carbon nanotubes. It is also believed that thermophysical measurement of a small carbon nanotube bundle will give direct evidence of nanomaterial decoration.

Finally, carbon nanotubes were grown by a chemical vapor deposition (CVD) and some nanotube bundles were successfully bridged on the suspended microdevice by using probe station with micromanipulator. Three thermoelectric properties, electrical conductance, thermopower, and thermal conductance, were measured in a cryostat under vacuum connected with several electronic instruments. Au nanoparticles were tried to be deposited by immersing the sample into Au salt due to a spontaneous reduction process on the nanotubes. Electrical conductance, thermal conductance, and thermopower increased with temperature, which is a typical trend presented in MWNTs. From difference in slope of thermal conductance and thermopower between pristine CNT and Au-CNT, it was found that a phonon scattering by Au nanoparticle decoration reduced a thermal conductance at a certain temperature or electron mobility as increase of temperature. As a result, *ZT* was higher in pristine CNT than Au-CNT, especially in higher temperature range. For the purpose of ZT enhancement, smaller and more nanoparticle decoration can be tried additionally or N type materials like Cu or Fe particles can be decorated on nanotubes in the future.

REFERENCES

1 Kim, D., Kim, Y., Choi, K., Grunlan, J. C. & Yu, C. H. Improved Thermoelectric Behavior of Nanotube-Filled Polymer Composites with Poly(3,4-ethylenedioxythiophene) Poly(styrenesulfonate). *ACS Nano* **4**, 513-523, doi:Doi 10.1021/Nn9013577 (2010).

2 Kim, Y. S., Kim, D., Martin, K. J., Yu, C. & Grunlan, J. C. Influence of Stabilizer Concentration on Transport Behavior and Thermopower of CNT-Filled Latex-Based Composites. *Macromolecular Materials and Engineering* **295**, 431-436, doi:DOI 10.1002/mame.200900243 (2010).

3 Yu, C., Kim, Y. S., Kim, D. & Grunlan, J. C. Thermoelectric Behavior of Segregated-Network Polymer Nanocomposites. *Nano Letters* **8**, 4428-4432, doi:Doi 10.1021/Nl802345s (2008).

4 Yu, C. H., Shi, L., Yao, Z., Li, D. Y. & Majumdar, A. Thermal Conductance and Thermopower of an Individual Single-Wall Carbon Nanotube. *Nano Letters* **5**, 1842-1846, doi:Doi 10.1021/Nl051044e (2005).

5 Appenzeller, J. Carbon Nanotubes for High-Performance Electronics - Progress and Prospect. *Proceedings of the IEEE* **96**, 201-211, doi:Doi 10.1109/Jproc.2007.911051 (2008).

6 Wu, Z. C., Chen, Z., Du, X., Logan, J. M., Sippel, J., *et al.* Transparent, Conductive Carbon Nanotube Films. *Science* **305**, 1273-1276 (2004).

7 Li, Z. R. *et al.* Polymer Functionalized N-type Single Wall Carbon Nanotube Photovoltaic Devices. *Applied Physics Letters* **96**, doi:Artn 033110 Doi 10.1063/1.3284657 (2010).

8 Jacobs, C. B., Peairs, M. J. & Venton, B. J. Review: Carbon Nanotube Based Electrochemical Sensors for Biomolecules. *Analytica Chimica Acta* **662**, 105-127, doi:DOI 10.1016/j.aca.2010.01.009 (2010).

9 Rowe, D. M. *CRC Handbook of Thermoelectrics*. CRC Press: Boca Raton, FL, 1995.

10 Mahan, G. D. & Sofo, J. O. The Best Thermoelectric. *Proceedings of the National Academy of Sciences of the United States of America* **93**, 7436-7439 (1996).

11 Yu, C. H., Ryu, Y., Yin, L. A. & Yang, H. Modulating Electronic Transport Properties of Carbon Nanotubes To Improve the Thermoelectric Power Factor via Nanoparticle Decoration. *ACS Nano* **5**, 1297-1303, doi:Doi 10.1021/Nn102999h (2011).

12 Blackburn, J. L., Barnes, T. M., Beard, M. C., Kim, Y. H., Tenent, R. C., *et al.* Transparent Conductive Single-Walled Carbon Nanotube Networks with Precisely Tunable Ratios of Semiconducting and Metallic Nanotubes. *ACS Nano* **2**, 1266-1274, doi:Doi 10.1021/Nn800200d (2008).

13 Dettlaff-Weglikowska, U., Skákalová, V., Graupner, R., Jhang, S. H., Kim, B. H., *et al.* Effect of SOCl2 Treatment on Electrical and Mechanical Properties of Single-Wall Carbon Nanotube Networks. *Journal of the American Chemical Society* **127**, 5125-5131, doi:Doi 10.1021/Ja046685a (2005).

14 Kong, B. S., Jung, D. H., Oh, S. K., Han, C. S. & Jung, H. T. Single-Walled Carbon Nanotube Gold Nanohybrids: Application in Highly Effective Transparent and Conductive Films. *Journal of Physical Chemistry C* **111**, 8377-8382, doi:Doi 10.1021/Jp071297r (2007).

15 Ryu, Y. T., Freeman, D. & Yu, C. G. High Electrical Conductivity and N-type Thermopower from Double-/Single-Wall Carbon Nanotubes by Manipulating Charge Interactions between Nanotubes and Organic/Inorganic Nanomaterials. *Carbon* **49**, 4745-4751, doi:DOI 10.1016/j.carbon.2011.06.082 (2011).

16 Sandler, J., Shaffer, M. S. P., Prasse, T.,Bauhofer, W., Schulte, K., *et al.* Development of a Dispersion Process for Carbon Nanotubes in an Epoxy Matrix and the Resulting Electrical Properties. *Polymer* **40**, 5967-5971 (1999).

17 Zhang, X. F., Sreekumar, T. V., Liu, T. & Kumar, S. Properties and Structure of Nitric Acid Oxidized Single Wall Carbon Nanotube Films. *Journal of Physical Chemistry B* **108**, 16435-16440, doi:Doi 10.1021/Jp0475988 (2004).

18 Agrawal, S., Raghuveer, M. S., Li, H. & Ramanath, G. Defect-induced Electrical Conductivity Increase in Individual Multiwalled Carbon Nanotubes. *Applied Physics Letters* **90**, doi:Artn 193104 Doi 10.1063/1.2737127 (2007).

19 Watts, P. C. P., Mureau, N., Tang, Z., Miyajima, Y., Carey, J. D., *et al.* The Importance of Oxygen-containing Defects on Carbon Nanotubes for the Detection of Polar and Non-polar Vapours through Hydrogen Bond Formation. *Nanotechnology* **18**, doi:Artn 175701 Doi 10.1088/0957-4484/18/17/175701 (2007).

20 Zhang, S., Ji, C., Bian, Z., Liu, R., Xia, X., *et al.* Single-Wire Dye-Sensitized Solar Cells Wrapped by Carbon Nanotube Film Electrodes. *Nano Letters* **11**, 3383-3387, doi:Doi 10.1021/Nl201790w (2011).

21 Ryu, Y. & Yu, C. H. The Influence of Incorporating Organic Molecules or Inorganic Nanoparticles on the Optical and Electrical Properties of Carbon Nanotube Films. *Solid State Communications* **151**, 1932-1935, doi:DOI 10.1016/j.ssc.2011.09.022 (2011).

22 Yu, C., Choi, K., Yin, L. & Grunlan, J. C. Light-Weight Flexible Carbon Nanotube Based Organic Composites with Large Thermoelectric Power Factors. *ACS Nano* **5**, 7885-7892, doi:Doi 10.1021/Nn202868a (2011).

23 Zhang, H., Cao, G., Wang, Z., Yang, Y., Shi, Z., *et al.* Carbon Nanotube Array Anodes for High-rate Li-ion Batteries. *Electrochimica Acta* **55**, 2873-2877, doi:DOI 10.1016/j.electacta.2010.01.028 (2010).

24 Marschilok, A., Lee, C. Y., Subramanian, A., Takeuchi, K. J. & Takeuchi, E. S. Carbon Nanotube Substrate Electrodes for Lightweight, Long-life Rechargeable Batteries. *Energy & Environmental Science* **4**, 2943-2951, doi:Doi 10.1039/C1ee01507a (2011).

25 Qu, L. T. & Dai, L. M. Substrate-enhanced Electroless Deposition of Metal Nanoparticles on Carbon Nanotubes. *Journal of the American Chemical Society* **127**, 10806-10807, doi:Doi 10.1021/Ja053479+ (2005).

26 Choi, H. C., Shim, M., Bangsaruntip, S. & Dai, H. J. Spontaneous Reduction of Metal Ions on the Sidewalls of Carbon Nanotubes. *Journal of the American Chemical Society* **124**, 9058-9059, doi:Unsp Ja026824t Doi 10.1021/Ja026824t (2002).

27 http://en.wikipedia.org/wiki/table_of_standard_electrode_potentials.

28 Liu, P., Sun, Q., Zhu, F., Liu, K., Jiang, K., *et al.* Measuring the Work Function of Carbon Nanotubes with Thermionic Method. *Nano Letters* **8**, 647-651, doi:Doi 10.1021/Nl0730817 (2008).

29 Zhao, J. J., Han, J. & Lu, J. P. Work Functions of Pristine and Alkali-metal Intercalated Carbon Nanotubes and Bundles. *Physical Review B* **65**, doi:Artn 193401 Doi 10.1103/Physrevb.65.193401 (2002).

30 Collins, P. G., Bradley, K., Ishigami, M. & Zettl, A. Extreme Oxygen Sensitivity of Electronic Properties of Carbon Nanotubes. *Science* **287**, 1801-1804 (2000).

31 Park, J. H. & Natesan, K. Oxidation of Copper and Electronic Transport in Copper Oxides. *Oxidation of Metals* **39**, 411-435 (1993).

32 http://en.wikipedia.org/wiki/copper.

33 Ebbesen, T. W., Lezec, H. J., Hiura, H., Bennett, J. W., Ghaemi, H. F., *et al.* Electrical Conductivity of Individual Carbon Nanotubes. *Nature* **382**, 54-56 (1996).

34 Anderson, P. A. The Work Function of Copper. *Physical Review* **76**, 388-390 (1949).

35 Eastman, D. E. Photoelectric Work Functions of Transition, Rare-Earth, and Noble Metals. *Physical Review B* **2**, 1-& (1970).

36 Chen, G. *Nanoscale Energy Transport and Conversion : A Parallel Treatment of Electrons, Molecules, Phonons, and Photons*. Oxford University Press: New York, NY, 2005.

37 Akai, Y. & Saito, S. Electronic Structure, Energetics and Geometric Structure of Carbon Nanotubes: A Density-functional Study. *Physica E-Low-Dimensional Systems & Nanostructures* **29**, 555-559, doi:DOI 10.1016/j.physe.2005.06.026 (2005).

38 Rogers, S. A. & Kaiser, A. B. Thermopower and Resistivity of Carbon Nanotube Networks and Organic Conducting Polymers. *Current Applied Physics* **4**, 407-410, doi:DOI 10.1016/j.cap.2003.11.060 (2004).

39 Su, W. S., Leung, T. C. & Chan, C. T. Work Function of Single-Walled and Multiwalled Carbon Nanotubes: First-principles Study. *Physical Review B* **76**, doi:Artn 235413 Doi 10.1103/Physrevb.76.235413 (2007).

40 Yang, S. B., Kong, B. S., Geng, J. & Jung, H. T. Enhanced Electrical Conductivities of Transparent Double-Walled Carbon Nanotube Network Films by Post-treatment. *Journal of Physical Chemistry C* **113**, 13658-13663, doi:Doi 10.1021/Jp903605p (2009).

41 Jackson, R., Domercq, B., Jain, R., Kippelen, B. & Graham, S. Stability of Doped Transparent Carbon Nanotube Electrodes. *Advanced Functional Materials* **18**, 2548-2554, doi:DOI 10.1002/adfm.200800324 (2008).

42 Kim, K. K., Bae, J. J., Park, H. K., Kim, S. M., Geng, H. Z., *et al.* Fermi Level Engineering of Single-Walled Carbon Nanotubes by $AuCl_3$ Doping. *Journal of the American Chemical Society* **130**, 12757-12761, doi:Doi 10.1021/Ja8038689 (2008).

43 Suzuki, S., Bower, C., Watanabe, Y. & Zhou, O. Work Functions and Valence Band States of Pristine and Cs-intercalated Single-Walled Carbon Nanotube Bundles. *Applied Physics Letters* **76**, 4007-4009 (2000).

44 Takenobu, T., Takano, T., Shiraishi, M., Murakami, Y., Ata, M., *et al.* Stable and Controlled Amphoteric Doping by Encapsulation of Organic Molecules inside Carbon Nanotubes. *Nature Materials* **2**, 683-688, doi:Doi 10.1038/Nmat976 (2003).

45 Braun, S. & Salaneck, W. R. Fermi Level Pinning at Interfaces with Tetrafluorotetracyanoquinodimethane (F4-TCNQ): The Role of Integer Charge Transfer States. *Chemical Physics Letters* **438**, 259-262, doi:DOI 10.1016/j.cplett.2007.03.005 (2007).

46 Chen, W., Chen, S., Qi, D. C., Gao, X. Y. & Wee, A. T. S. Surface Transfer P-type Doping of Epitaxial Graphene. *Journal of the American Chemical Society* **129**, 10418-10422, doi:Doi 10.1021/Ja071658g (2007).

47 Nosho, Y., Ohno, Y., Kishimoto, S. & Mizutani, T. The Effects of Chemical Doping with F(4)TCNQ in Carbon Nanotube Field-effect Transistors Studied by the Transmission-line-model Technique. *Nanotechnology* **18**, doi:Artn 415202 Doi 10.1088/0957-4484/18/41/415202 (2007).

48 Takano, T., Takenobu, T. & Iwasa, Y. Enhancement of Carrier Hopping by Doping in Single Walled Carbon Nanotube Films. *Journal of the Physical Society of Japan* **77**, doi:Artn 124709 Doi 10.1143/Jpsj.77.124709 (2008).

49 Hao, R., Qian, W., Zhang, L. H. & Hou, Y. L. Aqueous Dispersions of TCNQ-anion-stabilized Graphene Sheets. *Chemical Communications*, 6576-6578, doi:Doi 10.1039/B816971c (2008).

50 Dillon, E. P., Crouse, C. A. & Barron, A. R. Synthesis, Characterization, and Carbon Dioxide Adsorption of Covalently Attached Polyethyleneimine-functionalized Single-Wall Carbon Nanotubes. *ACS Nano* **2**, 156-164, doi:Doi 10.1021/Nn7002713 (2008).

51 Liao, K. S., Wang, J., Früchtl, D., Alley, N. J., Andreoli, E., *et al.* Optical Limiting Study of Double Wall Carbon Nanotube-Fullerene Hybrids. *Chemical Physics Letters* **489**, 207-211, doi:DOI 10.1016/j.cplett.2010.03.010 (2010).

52 Shim, M., Javey, A., Kam, N. W. S. & Dai, H. J. Polymer Functionalization for Air-stable N-type Carbon Nanotube Field-effect Transistors. *Journal of the American Chemical Society* **123**, 11512-11513, doi:Doi 10.1021/Ja0169670 (2001).

53 Wei, J. Q., Zhu, H. W., Jiang, B., Ci, L. J. & Wu, D. H. Electronic Properties of Double-Walled Carbon Nanotube Films. *Carbon* **41**, 2495-2500, doi:Doi 10.1016/S0008-6223(03)00295-1 (2003).

54 Shin, J. H., Shin, D. W., Patole, S. P., Lee, J. H., Park, S. M., *et al.* Smooth, Transparent, Conducting and Flexible SWCNT Films by Filtration-wet Transfer Processes. *Journal of Physics D-Applied Physics* **42**, doi:Artn 045305 Doi 10.1088/0022-3727/42/4/045305 (2009).

55 Sreekumar, T. V., Liu, T., Kumar, S., Ericson, L. M., Hauge, R. H., *et al.* Single-all Carbon Nanotube Films. *Chemistry of Materials* **15**, 175-178, doi:Doi 10.1021/Cm020367y (2003).

56 Zhang, D. H., Ryu, K., Liu, X., Polikarpov, E., Ly, J., *et al.* Transparent, Conductive, and Flexible Carbon Nanotube Films and Their Application in Organic Light-emitting Diodes. *Nano Letters* **6**, 1880-1886, doi:Doi 10.1021/Nl0608543 (2006).

57 Kong, J. & Dai, H. J. Full and Modulated Chemical Gating of Individual Carbon Nanotubes by Organic Amine Compounds. *Journal of Physical Chemistry B* **105**, 2890-2893 (2001).

58 Geng, H. Z., Kim, K. K., So, K. P., Lee, Y. S., Chang, Y. K., *et al.* Effect of Acid Treatment on Carbon Nanotube-based Flexible Transparent Conducting Films. *Journal of the American Chemical Society* **129**, 7758-+, doi:Doi 10.1021/Ja0722224 (2007).

59 Bower, C., Kleinhammes, A., Wu, Y. & Zhou, O. Intercalation and Partial Exfoliation of Single-Walled Carbon Nanotubes by Nitric Acid. *Chemical Physics Letters* **288**, 481-486 (1998).

60 Parekh, B. B., Fanchini, G., Eda, G. & Chhowalla, M. Improved Conductivity of Transparent Single-Wall Carbon Nanotube Thin Films via Stable Postdeposition Functionalization. *Applied Physics Letters* **90**, doi:Artn 121913 Doi 10.1063/1.2715027 (2007).

61 Dresselhaus, M. S., Dresselhaus, G. & Eklund, P. C. *Science of Fullerenes and Carbon Nanotubes*. Academic Press: San Diego, CA, 1996.

62 Harutyunyan, A. R., Pradhan, B. K., Chang, J. P., Chen, G. G. & Eklund, P. C. Purification of Single-Wall Carbon Nanotubes by Selective Microwave Heating of Catalyst Particles. *Journal of Physical Chemistry B* **106**, 8671-8675, doi:Doi 10.1021/Jp0260301 (2002).

63 Shim, H. C., Song, J. W., Kwak, Y. K., Kim, S. & Han, C. S. Preferential Elimination of Metallic Single-Walled Carbon Nanotubes Using Microwave Irradiation. *Nanotechnology* **20**, doi:Artn 065707 Doi 10.1088/0957-4484/20/6/065707 (2009).

64 Song, J. W., Seo, H. W., Park, J. K., Kim, J. E., Choi, D. G., *et al.* Selective Removal of Metallic SWNTs Using Microwave Radiation. *Current Applied Physics* **8**, 725-728, doi:DOI 10.1016/j.cap.2007.04.055 (2008).

65 Wang, L., Xiong, Y., Wu, Z., Duong, B., Seraphin, S., *et al.* Demetalization of Single-Walled Carbon Nanotube Thin Films with Microwave Irradiation. *Applied Physics a-Materials Science & Processing* **102**, 401-406, doi:DOI 10.1007/s00339-010-6069-2 (2011).

66 Lin, W., Moon, K. S., Zhang, S., Ding, Y., Shang, J., *et al.* Microwave Makes Carbon Nanotubes Less Defective. *ACS Nano* **4**, 1716-1722, doi:Doi 10.1021/Nn901621c (2010).

67 Hojati-Talemi, P. & Simon, G. Microwave-based Treatments for Multi-Walled Carbon Nanotubes. *Physica Status Solidi C - Current Topics in Solid State Physics, Vol 6, No 10* **6**, 2170-2173, doi:DOI 10.1002/pssc.200881725 (2009).

68 Kim, S. J., Park, Y. J., Ra, E. J., Kim, K. K., An, K. H., *et al.* Defect-induced Loading of Pt Nanoparticles on Carbon Nanotubes. *Applied Physics Letters* **90**, doi:Artn 023114 Doi 10.1063/1.2430993 (2007).

69 Shen, C., Brozena, A. H. & Wang, Y. H. Double-Walled Carbon Nanotubes: Challenges and Opportunities. *Nanoscale* **3**, 503-518, doi:Doi 10.1039/C0nr00620c (2011).

70 Ouyang, M., Huang, J. L., Cheung, C. L. & Lieber, C. M. Energy Gaps in "Metallic" Single-Walled Carbon Nanotubes. *Science* **292**, 702-705 (2001).

71 Brozena, A. H., Moskowitz, J., Shao, B., Deng, S., Liao, H., *et al.* Outer Wall Selectively Oxidized, Water-Soluble Double-Walled Carbon Nanotubes. *Journal of the American Chemical Society* **132**, 3932-3938, doi:Doi 10.1021/Ja910626u (2010).

72 Li, Z. R., Kandel, H. R., Dervishi, E., Saini, V., Biris, A. S., *et al.* Does the Wall Number of Carbon Nanotubes Matter as Conductive Transparent Material? *Applied Physics Letters* **91**, doi:Artn 053115 Doi 10.1063/1.2767215 (2007).

73 Dressel, M. & Grüner, G. *Electrodynamics of Solids : Optical Properties of Electrons in Matter*. Cambridge University Press: Cambridge, MA, 2002.

74 Dan, B., Irvin, G. C. & Pasquali, M. Continuous and Scalable Fabrication of Transparent Conducting Carbon Nanotube Films. *ACS Nano* **3**, 835-843, doi:Doi 10.1021/Nn8008307 (2009).

75 Ruzicka, B., Degiorgi, L., Gaal, R., Thien-Nga, L., Bacsa, R., *et al.* Optical and DC Conductivity Study of Potassium-doped Single-Walled Carbon Nanotube Films. *Physical Review B* **61**, R2468-R2471 (2000).

76 Hecht, D. S., Heintz, A. M., Lee, R., Hu1, L., Moore, B., *et al.* High Conductivity Transparent Carbon Nanotube Films Deposited From Superacid. *Nanotechnology* **22**, 075201, doi:Artn 169501 Doi 10.1088/0957-4484/22/16/169501 (2011).

77 Eklund, P. C., Holden, J. M. & Jishi, R. A. Vibrational-Modes of Carbon Nanotubes - Spectroscopy and Theory. *Carbon* **33**, 959-972 (1995).

78 Dresselhaus, M. S., Dresselhaus, G., Saito, R. & Jorio, A. Raman Spectroscopy of Carbon Nanotubes. *Physics Reports-Review Section of Physics Letters* **409**, 47-99, doi:DOI 10.1016/j.physrep.2004.10.006 (2005).

79 Goak, J. C., Lee, S. H., Han, J. H., Jang, S. H., Kim, K. B., *et al.* Spectroscopic Studies and Electrical Properties of Transparent Conductive Films Fabricated by Using Surfactant-stabilized Single-Walled Carbon Nanotube Suspensions. *Carbon* **49**, 4301-4313, doi:DOI 10.1016/j.carbon.2011.06.007 (2011).

80 Islam, M. F., Rojas, E., Bergey, D. M., Johnson, A. T. & Yodh, A. G. High Weight Fraction Surfactant Solubilization of Single-Wall Carbon Nanotubes in Water. *Nano Letters* **3**, 269-273, doi:Doi 10.1021/Nl025924u (2003).

81 Forney, M. W. & Poler, J. C. Sonochemical Formation of Methyl Hydroperoxide in Polar Aprotic Solvents and Its Effect on Single-Walled Carbon Nanotube Dispersion Stability. *Journal of the American Chemical Society* **132**, 791-797, doi:Doi 10.1021/Ja9085462 (2010).

82 Ausman, K. D., Piner, R., Lourie, O., Ruoff, R. S. & Korobov, M. Organic Solvent Dispersions of Single-Walled Carbon Nanotubes: Toward Solutions of Pristine Nanotubes. *Journal of Physical Chemistry B* **104**, 8911-8915 (2000).

83 Ramesh, S., Ericson, L. M., Davis, V. A., Saini, R. K., Kittrell, C., *et al.* Dissolution of Pristine Single Walled Carbon Nanotubes in Superacids by Direct Protonation. *Journal of Physical Chemistry B* **108**, 8794-8798, doi:Doi 10.1021/Jp036971t (2004).

84 Parra-Vasquez, A. N. G., Behabtu, N., Green, M. J., Pint, C. L., Young, C. C., *et al.* Spontaneous Dissolution of Ultralong Single- and Multiwalled Carbon Nanotubes. *ACS Nano* **4**, 3969-3978, doi:Doi 10.1021/Nn100864v (2010).

85 http://en.wikipedia.org/wiki/Methylpyrrolidone.

86 Nirmalraj, P. N., Lyons, P. E., De, S., Coleman, J. N. & Boland, J. J. Electrical Connectivity in Single-Walled Carbon Nanotube Networks. *Nano Letters* **9**, 3890-3895, doi:Doi 10.1021/Nl9020914 (2009).

87 Geng, H. Z., Lee, D. S., Kim, K. K., Han, G. H., Park, H. K. *et al.* Absorption Spectroscopy of Surfactant-dispersed Carbon Nanotube Film: Modulation of Electronic Structures. *Chemical Physics Letters* **455**, 275-278, doi:DOI 10.1016/j.cplett.2008.02.102 (2008).

88 Doherty, E. M., De, S., Lyons, P. E., Shmeliov, A., Nirmalraj, P. N., *et al.* The Spatial Uniformity and Electromechanical Stability of Transparent, Conductive Films of Single Walled Nanotubes. *Carbon* **47**, 2466-2473, doi:DOI 10.1016/j.carbon.2009.04.040 (2009).

89 Kymakis, E. & Amaratunga, G. A. J. Electrical Properties of Single-Wall Carbon Nanotube-Polymer Composite Films. *Journal of Applied Physics* **99**, doi:Artn 084302 Doi 10.1063/1.2189931 (2006).

90 Das, N. C., Liu, Y., Yang, K., Peng, W., Maiti, S., *et al.* Single-Walled Carbon Nanotube/Poly(methyl methacrylate) Composites for Electromagnetic Interference Shielding. *Polymer Engineering and Science* **49**, 1627-1634, doi:Doi 10.1002/Pen.21384 (2009).

91 Zhu, D., Bin, Y. Z. & Matsuo, M. Electrical Conducting Behaviors in Polymeric Composites with Carbonaceous Fillers. *Journal of Polymer Science Part B-Polymer Physics* **45**, 1037-1044, doi:Doi 10.1002/Polb.21115 (2007).

92 Kim, J. Y., Jung, J. H., Lee, D. E. & Joo, J. Enhancement of Electrical Conductivity of Poly(3,4-ethylenedioxythiophene)/Poly(4-styrenesulfonate) by a Change of Solvents. *Synthetic Metals* **126**, 311-316 (2002).

93 Narayanunni, V., Gu, H. & Yu, C. H. Monte Carlo simulation for investigating influence of junction and nanofiber properties on electrical conductivity of segregated-network nanocomposites. *Acta Materialia* **59**, 4548-4555, doi:DOI 10.1016/j.actamat.2011.04.001 (2011).

94 Romero, H. E., Sumanasekera, G. U., Mahan, G. D. & Eklund, P. C. Thermoelectric Power of Single-Walled Carbon Nanotube Films. *Physical Review B* **65**, doi:Artn 205410 Doi 10.1103/Physrevb.65.205410 (2002).

95 Yao, Q., Chen, L. D., Zhang, W. Q., Liufu, S. C. & Chen, X. H. Enhanced Thermoelectric Performance of Single-Walled Carbon Nanotubes/Polyaniline Hybrid Nanocomposites. *ACS Nano* **4**, 2445-2451, doi:Doi 10.1021/Nn1002562 (2010).

96 Geng, H. Z., Kim, K. K., Lee, K., Kim, G. Y., Choi, H. K., *et al.* Dependence of Material Quality on Performance of Flexible Transparent Conducting Films with Single-Walled Carbon Nanotubes. *Nano* **2**, 157-167 (2007).

97 Alvarez, L., Almadori, Y., Arenal, R., Babaa, R., Michel, T., *et al.* Charge Transfer Evidence between Carbon Nanotubes and Encapsulated Conjugated Oligomers. *Journal of Physical Chemistry C* **115**, 11898-11905, doi:Doi 10.1021/Jp1121678 (2011).

98 Kalbac, M., Farhat, H., Kavan, L., Kong, J. & Dresselhaus, M. S. Competition between the Spring Force Constant and the Phonon Energy Renormalization in Electrochemically Doped Semiconducting Single-Walled Carbon Nanotubes. *Nano Letters* **8**, 3532-3537, doi:Doi 10.1021/Nl801637h (2008).

99 Bourlon, B., Miko, C., Forro, L., Glattli, D. C. & Bachtold, A. Determination of the Intershell Conductance in Multiwalled Carbon Nanotubes. *Phys Rev Lett* **93**, doi:Artn 176806 Doi 10.1103/Physrevlett.93.176806 (2004).